DOE/ER/75786-3

FUEL EFFICIENT HYDRODYNAMIC CONTAINMENT FOR GAS CORE FISSION REACTOR ROCKET PROPULSION

Final Report

for Period September 30, 1992 - May 31, 1995

P. M. Sforza, and R. J. Cresci
Polytechnic University
Brooklyn, NY 11201

May 31, 1997

NOTICE

This report was prepared as an account of work sponsored by the United States Government. Neither the United States nor the Department of Energy, nor any of their employees, nor any of their contractors, subcontractors, or their employees, makes any warranty, express or implied, or assumes any legal liability or responsibility for the accuracy, completeness, or usefulness of any information, apparatus, product or process disclosed or represents that its use would not infringe privately-owned rights.

DISTRIBUTION OF THIS DOCUMENT IS UNLIMITED

Prepared for

THE U. S. DEPARTMENT OF ENERGY

Grant No. DE-FG02-92ER75786 - Amendment No. A001

DISCLAIMER

FUEL EFFICIENT HYDRODYNAMIC CONTAINMENT FOR GAS CORE FISSION REACTOR ROCKET PROPULSION

P. M. Sforza,* and R. J. Cresci†
Mechanical, Aerospace, and Manufacturing Engineering Department
Polytechnic University, Brooklyn, NY

Abstract

Gas core reactors can form the basis for advanced nuclear thermal propulsion (NTP) systems capable of providing specific impulse levels of more than 2000 sec., but containment of the hot uranium plasma is a major problem. The initial phase of an experimental study of hydrodynamic confinement of the fuel cloud in a gas core fission reactor by means of an innovative application of a base injection stabilized recirculation bubble is presented. The development of the experimental facility, a simulated thrust chamber approximately 0.4m in diameter and 1m long, is described. The flow rate of propellant simulant (air) can be varied up to about 2 kg/sec and that of fuel simulant (air, air-sulfur hexafluoride) up to about 0.2kg/sec. This scale leads to chamber Reynolds numbers on the same order of magnitude as those anticipated in a full-scale nuclear rocket engine. The experimental program introduced here is focused on determining the size, geometry, and stability of the recirculation region as a function of the bleed ratio, i.e. the ratio of the injected mass flux to the free stream mass flux. A concurrent CFD study is being carried out to aid in demonstrating that the proposed technique is practical .

---

*Professor
†Research Professor

Introduction

Time in transit is a major issue for interplanetary space exploration because exposure to space radiation and microgravity constitutes a health hazard for human crew members. To minimize flight time, high speed and therefore high thrust are required. At the same time, efficiency considerations demand low fuel consumption. The figure of merit for rocket propulsion systems is the specific impulse, defined as the thrust divided by the weight flow rate of fuel consumed. Fig. (1) compares the specific impulse achievable for chemical thermal propulsion (CTP), solid core nuclear thermal propulsion (SCNTP), and gas core nuclear thermal propulsion (GCNTP) systems.

Gas core fission reactors are seen to be capable of specific impulse levels on the order of 1500 to more than 2500 sec [Ref. 1]. Such performance is necessary for missions foreseen as part of interplanetary space exploration. Both open and closed cycle (light bulb) reactor designs have been considered and each has its own advantages. Our attention is focused on the open cycle reactor which is limited in practical realization by one fundamental problem: the containment of the uranium plasma. The containment must be one which minimizes the loss of the uranium fuel while reducing the thermal impact of the fuel on the structural components of the reactor chamber.

An innovative approach to dealing with this problem involves the transfer of technology from the field of projectile ballistics. A method of performance enhancement recently employed for ballistic projectiles is that of "base bleed". This is a technique whereby the base pressure is altered by injecting a small amount of gas through the base of the projectile into the recirculating flow region. The classical flow field just downstream of a flat base without injection is illustrated in Fig. 2 . As seen in this diagram there exists a recirculation region which is attached to the base with a stagnation point located on the base at the centerline. The bleed parameter, which is the ratio of mass flow injected into the base recirculation region to the mass flow in the surrounding free stream passing through an area equivalent to the total base area, is found to be on the order

of 10^{-2} or less for a stable recirculation zone [Ref. 3]. Uniform injection over the entire base surface causes the recirculation region to detach from the base as a bubble. In this state, which is illustrated in Fig. 3, the injected flow stabilizes the recirculation bubble by flowing around it, thereby buffering it from the outer shear layer, and proceeding downstream (e.g., Ref. 4). This is the basic mechanism we employ for the hydrodynamic containment of the fuel cloud in an open cycle gas core NTP system.

In the application of this concept to NTP the detached flow bubble contains the uranium plasma in a fashion which minimizes fuel losses and maintains its position remote from structural surfaces. The size of the bubble depends solely on the base dimension so that scaling for criticality is assured and effective radiant heating of the surrounding propellant is readily achieved. In the application of base bleed to projectiles it is sufficient to maintain a constant injection rate to meet the performance objectives desired. However, in the present NTP application such an approach would waste the fuel gas which stabilizes the fuel-laden bubble and passes on downstream. To optimize this process a periodic injection scheme is more appropriate. The sequence of events envisaged in an operational rocket system is as follows:

(a) At the outset there is no injection and the propellant flows around the base and within the attached recirculation region.

(b) A high rate of fuel injection is initiated through the base which replaces the recirculation region with a jet of pure fuel gas.

(c) The fuel rate is modulated to permit the reformation of a recirculation bubble which, now, however, contains pure fuel.

(d) Additional injected fuel merely flows around the bubble and is lost downstream and it is at this point that fuel injection is terminated.

(e) Immediately thereafter the injectant is switched to propellant to provide the stabilizing flow around the fuel bubble while absorbing radiation as it flows on downstream to the nozzle.

(f) During the entire process the main propellant flow around the outside of the base is continually absorbing heat and ultimately provides the major thrust of the rocket.

(g) As time progresses diffusion depletes the quantity of uranium gas in the bubble and when this reaches some predetermined level the propellant injection is terminated and steps (b) through (f) are repeated.

The overall research program introduced in this paper is aimed at experimental and computational investigation of the feasibility of the hydrodynamic containment scheme described above. The test facility is described first, followed by the results obtained in an experimental investigation of fuel/propellant recirculation regions using air/air (as in Ref. 5). The aim of the project initiated here is to ultimately provide data on the following issues:

(a) The size, geometry, and stability of the recirculation region as a function of the bleed ratio, i.e. ratio of injected mass flux to free stream mass flux.

(b) The effect of the bleed ratio on the attachment and detachment of the recirculation region.

(c) The maximum bleed ratio attainable prior to complete blow-off of the recirculation region, i.e. loss of a stable recirculating flow.

Sizing and Simulation Performance of Test Facility

Flow simulation requirements

To simulate the flow field in the thrust chamber of a prototype rocket like that illustrated in Fig. 4 (Refs. 6 and 7) an appropriate test facility was designed. Here prototype refers to a full scale gas core reactor engine as reported by Gurfink (Ref. 8) and summarized in Table 1. In order to ensure proper simulation the model and prototype must be both geometrically and dynamically similar. This means that the model reactor must satisfy a range of prototype reactor characteristics, such as various geometric aspect ratios, and of hydrodynamic parameters, such as Reynolds number. In addition it was required that the model dynamic performance must be within the capabilities of the existing air supply system. The model reactor characteristics and flow conditions ultimately employed are summarized in Table 2. An additional consideration in the design process was minimization of both expense and manufacturing time through the use of standard parts, materials, and processes.

Test Model Characteristics

Geometric similarity requires that the model and prototype be the same shape, and that all linear dimensions of the model be related to corresponding dimensions of the prototype by a constant scale factor. By examining various diameter combinations of standard steel piping it was found that a 0.41m (16 inch) outside diameter (OD) pipe with a 0.39m (15.25 in.) inside diameter (ID) for the test model and a 0.27m (10.75 inch) base diameter (D) provide reasonable best geometric scale combinations, as shown below:

		Prototype	Test Model
Chamber diameter ratio	ID/D	1.3	1.4
Annulus width ratio	d/D	0.14	0.2
Length ratio	L/D	1.0	1.0

The corresponding annulus width for the model, d = 57mm (2.25 inches). The characteristic length L of the fuel cloud is approximately equal to the diamter D of the recirculation bubble.

The condition for dynamic similarity between geometrically similar flows is expressed in terms of the Reynolds number

$$Re=w_aD/\nu$$

where the average velocity through the annulus is

$$w_a=Q/A_a$$

and Q is the volumetric flow rate through the annulus, which has the cross-sectional area A_a.

Gurfink (Ref. 8) indicates a range of prototype Reynolds numbers from 10^5 to 10^7. The lower limit, 10^5, is preferred for the test model in anticipation of lower velocities (easy to measure), lower mass flow rates (easily achieved with existing air supply system), and longer run times before refilling of air tanks is required.

In order to obtain a value for the average velocity in the annulus region it is necessary to estimate the nominal density of air flowing in this region. This is done by choosing an appropriate operating pressure and temperature of the air in the test section, and then use the ideal gas law to determine density. Assuming that the net heat transfer rate across the test model wall is negligible and the velocity is low, it is reasonable to expect an air temperature equal to the ambient test room temperature which is about 294K (529R). Furthermore, by assuming an operating pressure of 2 atmospheres, the density of air in the test section is found to be approximately 0.076 kg/m^3 (0.167 lbs/ft^3). The average velocity in the annulus region is found to be approximately 12m/s (39 ft/s).

It should be noted that the object of this investigation is not to generate thrust from the engine simulator, but rather to simulate the choked throat in the rocket. As a result the test model nozzle is of a converging axisymmetric type, as shown in Fig. 5. An expression for calculating the required nozzle throat diameter, given the stagnation conditions, is as follows:

$$D^* = [2.4mT_0{}^{0.5}/P_0\,]^{0.5} \qquad (1)$$

where the stagnation temperature, T_0, stagnation pressure, P_0, and the mass flow rate $m=\rho Q$, are known. The mass flow rate through the nozzle must be the same as the mass flow rate through the annulus, in order to satisfy conservation of mass. As a result Eq. 1 can be rewritten in terms of annulus properties, from which the required nozzle throat diameter is determined to be 69mm (2.7 inches).

Since it is preferable to use standard tube diameters in order to avoid unnecessary manufacturing, the nozzle throat diameter was increased to the next standard size, 76mm (3 inches). Consequently, according to Eq. 1, a change in mass flow rate is required to achieve sonic flow in the nozzle throat, keeping all other variables the same. The resulting mass flow rate value changes the nominal average velocity in the annulus region from 12 m/s (39 ft/s) to 15 m/s (49 ft/s). The new value for the Reynolds number of 5.75×10^5, which is still in the range given by Ref. (8). A summary of test model characteristics is given in Table 2.

Air Supply System Requirements

The test model is attached to the existing air supply system via a 76mm (3 inch) diameter pipe which feeds from the low pressure side of a 76mm hydraulically operated globe valve. The pipe is 5.5m (18 feet) in length and s rated at 4.1 MPa (600 psia).

Under these circumstances it is of interest to find certain operating conditions, such as pressure upstream of the valve, valve setting, and maximum pressure in feed line, which are necessary to obtain the required dynamic performance in the test model, and compare these values with the limits imposed by the existing air supply system. This task is performed by examining the pressure loss through the piping system due to frictional effects.

The problem, which is schematically illustrated in Fig. 6, is modeled as a one-dimensional Fanno flow to estimate the effects of friction on pressure, temperature, and velocity. It is assumed that the flow velocity at the end of the feed line is sonic and that a normal shock wave resides at the entrance of the line. Under these conditions, pressure and temperature reach their

maximum values after the normal shock. These extreme values are of interest for comparison with the limiting values of the existing air supply system.

Local stagnation pressure, P_0, in the pipe is given as function of the local Mach number and $\gamma = 1.4$ by the following expression:

$$P_0/P_0^* = (2 + 0.4M^2)/13.82M \tag{2}$$

where P_0^* is the stagnation pressure at the end of the pipe under the assumption of sonic flow at this location. The value for this pressure can be assumed to be 2 atm, which is the required stagnation pressure in the test section of the simulator. As previously mentioned it is necessary to find the pressure after the normal shock, and as a result the local Mach number in Eq. 2 becomes the Mach number after the normal shock, M_2 in Fig. 6, which, according to normal shock theory, must be subsonic. An expression which relates the Mach number at the entrance of the pipe to the length of the pipe under the assumption of sonic flow at the end of the pipe is as follows:

$$4fL^*/D = (1-M^2)/1.4M^2 + (6/7)\log_e[1.2M^2/(1 + 0.2M^2)] \tag{3}$$

where L^* and D are the length and diameter of the pipe, respectively, and f is the average friction coefficient for the pipe, assumed to be equal to 0.005. The Mach number after the normal shock, M_2, is found to be 0.46 from Eq. 3. Then using Eq. 2 the stagnation pressure, P_{02} in Fig. 6, is calculated to be 3atm, well under the rated pressure of 40atm.

It is now possible to estimate the pressure conditions upstream of the valve, the side of the valve connected to the air storage facility. The Mach number upstream of a normal shock is related to the Mach number after the shock by the following relation:

$$M_2 = [(1 + 0.2M_1^2)/(1.4M_1^2 - 0.2)]^{0.5} \tag{4}$$

where M_1 is the Mach number ahead of the shock and M_2 is 0.46. From Eq. 4 M_1 is found to be 3.3. The local stagnation pressure, P_{01}, ahead of the normal shock is given as a function of the local Mach number, M_1, and the stagnation pressure, P_{02}, after the shock by the following expression:

$$P_{01}/P_{02} = [(7M_1^2 - 1)/6]^{2.5} [(1 + 0.2M_1^2)/1.2M_1^2]^{3.5} \quad (5)$$

Eq. 5 gives a value for P_{01} of 1.17 MPa (170 psia), and assuming an isentropic expansion through the valve, the stagnation pressure is constant in all regions ahead of the normal shock shown in Fig. 6. Therefore the pressure in the air storage facility, P_0 in Fig. 6, should be at least 1.17 MPa. This level is easily achieved with the existing facilities, which are illustrated in Fig. 7 and described in more detail in Appendix A.

Test Facility

The original test facility

The physical arrangement of the original test facility design (Ref. 9) is shown in Fig. 8. A vertical flow facility was chosen to minimize buoyancy effects during variable density test runs and to optimize use of floor space. In this set-up air flows vertically downward through a long 76mm (3 in) pipe. The air then turns through 90^{o}, becoming horizontal. After passing through a 1.22m (4 ft) long horizontal section of 76mm (3 in) pipe the high velocity air turns through another 90^{o} upward so that it now travels vertically. The next section is a 0.75m (29.6 in) long conical diffuser which expands the pipe to a final diameter of 0.41m (16 in). This slows the flow speed down to about 7.6 m/s (25 ft/s) at the diffuser exit. The last 0.15m (6 in) of the diffuser encloses a smooth, wooden, 0.27m (10.75 in) diameter hemisphere which is centered along the pipe axis. This hemisphere begins the smooth transition to the annular region. The annulus has, for its inner wall, a 0.27m (10.75 in) diameter hollow cylindrical section while a 0.41m (16 in) pipe with an inner diameter of 0.39m (15.25 in) forms its outer wall. This hollow centerbody forms a 57mm (2.25 in) annulus through which the flow travels and is supported by three streamline struts through which the injectant may be introduced. The annulus reduces the flow area which increases the velocity to a nominal value of 15m/s (50 ft/s) according to the incompressible flow continuity equation. A circular plate, either solid or porous, is set on top of the centerbody and defines the entrance to the test section. The test section proceeds at a constant diameter for 0.57m (22.5 in) and ends in a 45^{o} convergent nozzle with a 76mm (3 in) throat. The air then expands freely into a 0.25m (10 in) pipe, turns through another 90^{o}, and exhausts to the ambient atmosphere outside the test building. This flow path may be more easily visualized by viewing the cutaway view of the facility presented in Fig. 9. The simulated propellant (air) flow enters from beneath the floor, decelerates through the diffuser (6) and flows around the center body (16). The simulated fuel (air or foreign gas) is injected through the porous base of the center body (17) to establish the recirculation bubble in the test section (3)

where flow measurements are made thorugh the windows. The propellant gas (along with a small quantity of simulated fuel) then travels downstream through the throat (11) and is finally exhausted into the atmosphere. The completed test facility, as originally constructed, is shown in the photograph in Fig. 10. Preliminary tests in this facility indicated that the flow over the centerbody was not sufficiently axisymmetric to warrant extensive flow surveys; this will be described in the following section. In order to improve the flow quality the facility configuration was changed.

The improved test facility

The facility was redesigned (Ref. 10) using many of the same sections as the original design and is illustrated in Fig. 11. In this improved set-up high subsonic velocity air flows downward through a 0.76m (30 in) section of 76 mm (3 in) pipe and enters the conical diffuser described previously. This slows the flow down to 7.6m/s (25 ft/s) before it makes two 90^{o} turns through standard elbow sections and ends up flowing vertically toward the test section. The flow then enters a flow conditioning section composed of 0.178m (7 in) long by 31.8mm (1.25 in) diameter aluminum tubes packed together and bounded on each end by a woven wire cloth square mesh screen measuring 12.7mm x 12.7mm (0.5 in x 0.5 in) with a porosity of 0.764 and a wire diameter of 1.6mm (0.0625 in). Beyond the flow conditioner the flow proceeds for another 0.61m (24 in) prior to encountering the nose of the centerbody. Thereafter the test facility is identical to that described previously. These changes were made in the facility in order to improve the axisymmetry of the flow and to reduce the turbulence in the annulus region. A photograph of the new rig is shown in Fig. 12.

The porous base plate injection system

A simple system for injection of the simulant fuel through the porous base was designed and is shown schematically in Fig. 13. An air (or foreign gas) supply line was fitted with two valves, an isolation valve to separate the system from other projects and a regulator valve to

control the upstream pressure. The flow rate was measured with an orifice plate designed according to ASME standards. The outer diameter of the orifice plate measured 9.5mm (0.375 in) and the inner diameter 4.8mm (0.1875 in) for a diameter ratio of 0.5. Downstream of the orifice plate the flow entered a 25.4mm (1 in) steel manifold with three branches each carrying approximately 1m (39 in) of 12.7mm (0.5 in) copper tubing. These tubes terminated in fittings mating them to the 7.1mm (0.28 in) inside diameter injection ports passing through the three symmetrically placed streamlined struts supporting the centerbody in the test section. The maximum bleed rates achievable with the system described was around 6%.

The gas metered into the centerbody could only escape through randomly spaced 100 μm pores in the 2.4mm (0.093 in) thick base plate constructed of sintered stainless steel powder supplied by Mott Metallurgical Corporation. The base plate was attached to the centerbody by sandwiching it between the centerbody and a 0.27m (10.75 in) outside diameter retaining ring 12.7mm (0.5 in) wide and 3mm (0.125 in) thick and then fastening the ring to the wall of the centerbody with eight small screws.

Instrumentation and data acquisition

A pitot pressure rake was employed to gather data at the annulus, as shown in Fig. 14, and in the shear layer surrounding the recirculation region. The pitot rake, shown in Fig. 15, has five 1.6mm (0.063 in) diameter steel tubes set up 11.1mm (0.44 in) apart on centers so that the span between the centers of the first and fifth tubes is 44.5mm (1.75 in). The rake support, a 9.5mm (0.375 in) diameter aluminum tube, measured 0.61m (2 ft) in length so as to be capable of extending completely across the test section. Each of the pitot tubes extended out from the support tube a distance of 22.2mm (0.875 in) and were coupled to transducers by appropriate lengths of Tygon tubing.

A short-tipped Dwyer pitot-static tube was used to measure mean velocity throughout the experiments reported here. The dimensions of this probe are as follows: tip length = 46mm (1.81

in), stem length = 0.33m (13 in), and four evenly spaced static taps 12.7mm (0.5 in) behind the probe tip.

The total pressure rake and pitot-static probe could be introduced into the test section were through three windows located 90^{o} apart around the circumference of the test section. These windows, labeled A, B, and C, measured 0.28m (11 in) high, 63mm (2.75 in) wide, and 50mm (2 in) deep. Pyrex glass panes were used for viewing the test section while aluminum window plates were used for mounting the rake and the probe. An aluminum frame with a rubber gasket and 12 screws secured the window plates to the structure. Window B was located on the outer side of the U-shaped facility and windows A and C were located 90^{o} to either side of B while site D, directly opposite B identified the location of a virtual window on the inner side of the U.

In addition, another pitot probe was installed in the "rocket nozzle" throat downstream of the thrust chamber. This was used in conjunction with a static tap in the throat region to obtain the throat Mach number. Data taken during shake-down runs of the facility indicated that the throat was in fact choked over the range of mass flow rates tested. As previously shown in Table 2, the design stagnation pressure is two atmospheres. Tests were run at 1.5, 2.0, and 3.0 atmospheres and the throat remained choked under all test conditions. The annulus pitot pressure varied in proportion to the stagnation pressure in the thrust chamber.

Validyne differential pressure transducers (model DP-7) and signal amplifiers were used to measure pressure differentials. Their range was $\pm$10mmHg ($\pm$1.4kPa or $\pm$0.2psid) with an uncertainty of $\pm$6.9Pa or $\pm$0.001psid). Kulite absolute pressure transducers (model ITQ-50) and signal amplifiers were used to measure absolute pressures. Their specified range was 345kPa (50 psia) with an uncertainty of $\pm$1.7kPa ($\pm$0.25 psia).

The scheme used to measure pitot pressure with the rake is shown schematically in Fig. 15. The pressure output line from the rakes fifth tube was split so that one side would enter one differential pressure transducer while the other would lead to an absolute pressure transducer. This absolute reading serves as the reference pressure for the four other adjacent pressure

readings. The lines from the four remaining tubes were split as needed to obtain the differential pitot pressures between two adjacent tubes, In this fashion, the measurement system is closed. Along with the reference absolute pitot pressure, the pitot pressure profile across the entire rake could be constructed. Measurement accuracy is thereby determined by the accuracy and calibration of the pressure transducers.

The tunnel static pressure, measured at a wall tap located 0.22m (8.6 in) upstream of the base is simultaneously recorded using an absolute pressure transducer. This pressure is assumed to be constant for all regions of nearly parallel flow, e.g. within the annulus and in the outer portions of the subsequent shear layer, and was used in conjunction with the pitot rake readings to deduce the velocity in such regions by means of the incompressible form of the Bernoulli equation. In the recirculation region itself there may be substantial streamline curvature and the single pitot-static tube was used to measure velocities. Since there is also a flow reversal in that region the probe tip had to be properly aligned with the flow. With these two approaches it was possible to develop velocity profiles throughout most of the region of interest.

For all runs, the data acquisition system was started manually once the wall static pressure steadied out at the nominal value of 2 atmospheres. A DAS-16 data acquisition board on a CompuAdd 286 computer was used to record all data with typical run times being set at 5 seconds. This run time was set after determining that the mean pressures measured varied no more than 1% for runs of 5 seconds or longer. Sampling occurred at a rate of 100 samples per second per channel for all runs. Appendix A includes further details concerning the data reduction schemes employed.

Experimental Results and Discussion

Flow field quality and facility design

For the current phase of the study the experimental simulation of fuel/propellant recirculation regions using air/air (as in Ref. 5) has been performed in order to determine the size, geometry and stability of the recirculation region as a function of the bleed ratio, including complete blow-off of the recirculation region.

After shake-down runs in the original facility, detailed measurements were carried out at windows A, B, and C in the annulus at the plane of the base (z/D = 0) and at a typical downstream location (z/D = 0.82) to assess flow quality (Ref.11). As can be seen in Figs. 16 and 17, the velocity distributions both in the annulus and at the downstream station show substantial asymmetries. This deviation from axial symmetry is believed to be caused by the flow turning in the elbows of the air supply line before entering the diffuser upstream of the annulus. In addition, the relative intensity estimated from the pressure measurements approached 100% at several locations. Due to the asymmetric and turbulent behavior of the flow in the base region (including the annular flow) the facility configuration was altered to eliminate the high velocity in the 90^{o} elbows and to reduce turbulence levels thereby improving the symmetry in the test region. This altered design, which was described previously and illustrated in Fig. 11, did produce a much more nearly axisymmetric flow and reduced turbulent intensities by factors of up to four. All further measurements described in the present report were obtained with the new configuration and are discussed below.

Velocity profiles with zero base bleed

Velocity profiles were measured for the case of a solid base plate, i.e. no base bleed, at three stations for each of the four window locations. Results for the flow in the annulus at the plane of the base, z/D = 0, are shown in Fig. 18. It is clear that the flow is quite symmetric at locations A, B, and C, with some noticeable deviation at location D. Since this location has no

window, the profile there was taken by extending the pitot rake completely across the test section from its support window at location B. There is therefore still some slight, but measurable effect of the U-turn the flow has negotiated far upstream. Profiles across the entire test section for two downstream locations, z/D = 0.40 and 0.82, are shown in Figs. 19 and 20, respectively. Since the z-coordinate is considered positive in the downstream direction, the velocities are also considered positive in that direction. The reverse flow velocities were measured by manually traversing the pitot-static tube so only sites A, B, and C are shown, while the positive velocities were measured with the pitot rake, as described previously.

Centerline velocity distribution with zero base bleed

Velocity measurements were taken along the centerline from the solid base plate (z/D=0) through the recirculation region at five axial locations. The results, normalized by the average velocity through the annulus, w_a, are shown in Fig. 21. The maximum velocity ratio was 0.43 and occurred at z/D = 0.67 while extrapolation of the data indicated that the rear stagnation point was located at z/D= 1.13. Comparisons with several other investigators are also shown in Fig. 21, two for subsonic annulus flow, Lightman and Magill (Ref. 12) and Porteiro, et al (Ref. 13), and one for supersonic annulus flow, Dutton et al (Ref. 14). None of these references had a downstream throat in their facilities. All the investigations, including the present one, suggest a recirculation region of diameter and length both on the order of the base diameter.

The velocity distribution along the centerline was measured again, this time with the porous base plate installed but with no injection. It was considered important to evaluate the effect of any motion of the air within the centerbody through the porous base during the test period. As can be seen from Fig. 22, the differences are very small, with the largest differences occurring near the rear stagnation point where the velocity is approaching zero.

Centerline velocity distribution with base bleed

Velocity measurements along the centerline starting from the plane of the base (z/D = 0) for bleed rates N = 2.5% and 5% are shown in Fig. 23. Also shown are the results for zero bleed, N =0, as well as the results of Porteiro et al (Ref. 13) for N = 3.28%. Polynomial curve fits through the data have been added for clarity. In general, there is a trend of moving the rear stagnation point further downstream as the bleed rate is increased and, similarly, the front stagnation point moves off the body and on downstream as well. Thus the recirculation region behaves like a self-contained bubble moving off the body a distance of 10% to 20% of the base diameter for relatively small injection rates. The present results may be summarized as follows:

Bleed rate (N%)	Front stagnation point, z/D	Rear stagnation point, z/D
0	0	1.13
2.5	0.04	1.22
5.0	0.10	1.28

Velocity profiles with base bleed

Velocity profiles across the test section were measured at two downstream locations, z/D = 0.40 and 0.82, for two window locations, B and C, and two bleed rates, N = 2.5% and 5%. Results are shown in Figs 24 through 27 and illustrate close correspondence to the case of zero base bleed. An assessment of the extent of axisymmetry achieved in these cases with injection may be achieved by viewing Figs. 28 through 31. These show results for locations B and C on the same figure with polynomial curve fits through the data added for clarity. There is reasonable evidence of symmetry with the largest discrepancies appearing in the shear layer, the region where velocity measurements are less reliable.

Estimated streamline patterns in the recirculation region

The dividing streamline provides the demarcation between the mass trapped inside the recirculation bubble and the mass flowing around it on its way out through the nozzle throat.

Therefore, by continuity, the mass flow between the test section wall and the dividing streamline is equal to the mass flow through the annulus plus the mass flow injected through the base. Integration of the velocity profiles thus far obtained across the test section, assuming incompressible flow, thus provides a means to locate the dividing streamline.

Mass flow distributions as a function of radius were calculated by profile integration for each reported axial station and window location. The curves obtained at the different window sites were then averaged to provide a single mass flow distribution for each z/D location. To account for inevitable inaccuracies in the total mass flow results between stations, each distribution was normalized to its own calculated mass flow so that the maximum mass flow at any station was unity. Then it is a simple matter to construct streamlines by merely connecting up points with the same mass flow ratio.

The data obtained in the present study yields a maximum of four points to connect up in order to sketch approximate streamline patterns in and around the recirculation bubble: the two stagnation points and the two intermediate locations, z/D = 0.40 and 0.82. In addition, the flow curvature encountered in the recirculation region limits the accuracy achievable with the instrumentation used. Therefore the flow patterns illustrated in Figs. 32 to 34 must be considered merely as estimates of the actual flow fields, especially in regions of high curvature. However, it does seem clear that the bubble diameter is close to that of the base plate and the effect of uniform injection is to lift the bubble off the base without disturbing its integrity.

Theoretical Analysis

A numerical study of the test facility has been conducted using a time dependent compressible Full Navier-Stokes (FNS) computer code (VNAP2, Ref. 15). The intent of the study was to investigate the effects of the proximity of the downstream nozzle and base bleed rate on the characteristics and location of the recirculation bubble.

Various numerical studies of base flow and base-bleed are reported in the literature, but most concentrate on supersonic and transonic flow as they apply to free flight of projectiles. Refs. (16) and (17) describe the development and application of a thin shear layer Navier-Stokes code to the base region of such projectiles with particular emphasis on base drag reduction. Low speed studies often pertain to bluff body flame stabilization in gaseous combustors, as reported in Refs. (18) through (20). None of the numerical (and experimental) studies, of which the current authors are aware, consider the effects of a converging-diverging nozzle in the vicinity of the recirculation bubble. Concern over the possible effects center around issues related to stability and shape of the bubble. These parameters are of importance when considering the unsteady diffusion of nuclear fuel and the preservation of a recirculation bubble capable of containing the critical mass of fuel.

The computational mesh used for the current study consisted of 4300 grid points and is depicted in Fig. 35 and an axisymmetric formulation of the equations of motion is employed. The left boundary is made up of the annular propellant flow region and the base region. Since the right side or outflow boundary is supersonic, the exit pressure of the flow at the exit plane is calculated by the code. This eliminates the usual problem of prescribing the downstream pressure necessary for the case of subsonic outflow (ie. a fully elliptic problem). Sensitivity to this boundary condition has been shown to be of critical importance in numerical solution of problems of this nature.

Although the computer code utilized here has the capability for full viscous simulation including zero, one, and two equation turbulence closure models, our initial analyses were at the

Euler level. General features and trends associated with the fluid dynamics of the flow were extracted so as to facilitate more accurate solutions at a later time. Due to the small time steps required to resolve the subsonic portions of the flow, computer run times on the order of six hours on a SUN SparcStation 10 were typical for these inviscid cases. Figure 36 depicts a velocity vector plot for a case with zero injection through the base. As expected, a recirculation bubble is generated with a downstream stagnation point located at a distance of approximately one base diameter from the base. As is evident from the figure, the effect of the downstream pressure gradient appears to be negligible in this case which corresponds to the current geometry of the test facility.

The effect of a small amount of base injection (bleed rate = 2% and 4%) can be seen from Figs. 37 and 38. The bubble forms away from the base with two centerline stagnation points. As expected, the location of the downstream stagnation point is close to that in the case without base bleed. This phenomena has been observed in the experiments reported here. In the calculations the bubble is found to be displaced from the base by a distance roughly equal to 20% of the base diameter.

For all of the above cases, the following procedure was used to obtain the results shown. First, a computational mesh was generated to model the flow field from the base to the station where the downstream nozzle begins converging. The upstream boundary condition was modelled as high velocity inflow in the annular region and zero (or very low) velocity inflow in the base region. The downstream boundary, subsonic for these cases, had a prescribed uniform pressure. An initial data plane was generated using a separate computer program whose output was read into the VNAP2 code. This initial data plane consisted of a triangular region of zero velocity whose vertices are the center of the base, the edge of the base, and on the centerline of the flow at a distance of one base diameter downstream of the base. The purpose of this was to "jump-start" the solution of the recirculation bubble. The remainder of the flow field was calculated using one-dimensional isentropic flow starting with the flow in the annulus.

These base region only (no nozzle) cases were run for each base injection rate for approximately 25,000 time steps (0.25 seconds). Solutions began to diverge at approximately 30,000 time steps, typically on the centerline downstream of the second stagnation point and/or at the edge of the base where a large velocity gradient exists. Numerous modifications to the local grid spacing and boundary conditions were attempted, however none were successful. Nevertheless, the solution planes after 25,000 time steps revealed a reasonable-looking recirculation bubble and indicated a conservation of mass at each axial station within 5%. These solution planes were saved in a data file.

Converging-diverging nozzle cases were also run separate from the base region cases. The geometry here represented the portion of the flow field downstream of the initial convergence. The upstream boundary condition here was total temperature and pressure, and mass flow. The VNAP2 code, being originally written to compute subsonic-to-supersonic nozzle flows, had no trouble obtaining a converged solution here. The results of the nozzle cases, each corresponding to the total mass flow associated with the combined annular flow and base injection were saved in a data file.

At this point the solution planes from the base region only and nozzle-only runs were read into the VNAP code utilizing a computational mesh which merged the two flow fields (Fig. 10). The results shown in the subsequent figures correspond to the solution after approximately 25,000 time steps (approximately 0.1 seconds). Since the initial (time=0) flow field was generated in the manner described (patching of previous solutions) this obviously does not correspond to "real" time. Divergence of the solutions occurred consistently at approximately 30,000 time steps at the same regions as in the base flow-only runs. Again numerous techniques including time and space smoothing, grid refinement, and adjustment of boundary conditions were unsuccessfully attempted to mitigate the numerical instability.

After exhausting the capabilities of the VNAP2 code, a commercial, well established, FNS code was utilized to attempt to solve this axisymmetric base region problem. Numerical instability again precluded the attainment of any solutions. It appears that the solution of the

nearly-incompressible base flow problem is quite difficult numerically. It is possible that the problem must be modelled fully in three dimensions to eliminate recirculating flow streamlines from focussing on the centerline, a result of the axisymmetric assumption. Two-dimensional (planar) cases were run and were found to be more stable, however no runs progressed to "steady-state".

Conclusions

A new approach for achieving fuel efficient hydrodynamic containment in a gas core nuclear rocket has been presented and exploratory experimental and computational studies of this new scheme have been described. The proposed mechanism confines the fuel plasma within a base injection stabilized recirculation region. This flow region is displaced from contact with any structural members by means of small amounts of injection through a base plate, thus promising improved heat protection in addition to fuel containment. The major results of the present program are as follows:

a) A laboratory facility which can properly simulate the hydrodynamics of a full-scale gas core nuclear rocket using the proposed fuel containment scheme has been constructed and operated.

b) Air injection through a porous plate at a mass flow rate up to 5% of that in the surrounding main flow detaches and stabilizes a stable recirculation bubble. The detachment distance is on the order of 10% to 20% of the bubble diameter. The bubble diameter and length are approximately equal to the diameter of the base through which injection takes place .

c) The presence of a sonic thoat less than two base diameters downstream of the base injection region, which would be the case for a practical thrust chamber, does not hamper the formation or retention of the recirculation bubble.

Future experiments will deal with establishing the rate of diffusion into and out of the bubble by using a foreign gas as the injectant and measuring its concentration as a function of time. Studies involving flow field mapping of the bubble as a function of base flow injection rate are continuing (Ref. 21).

Despite the promising results obtained in the present study, more work is needed to address the following important concerns:

a) The effects of temperature and its gradients on mean flow characteristics

b) The effects of vehicle accelerations on the recirculation region

c) The effects of time varying injection which is required for best performance

d) The extent of thermal protection offered by the detached plasma bubble

References

1. Schwenk, F.C. and Franklin, C.E.: "Comparison of Closed and Open Cycle Systems", NASA SP-236, Research on Uranium Plasmas and Their Technological Applications", Jan. 1970, pp. 3-12.
2. Sahu, J., Nietubicz, C.J., and Steger, J.L.: "Navier-Stokes Computations of Projectile Base Flow With and Without Mass Injection", AIAA Jl, Vol. 23, No. 9, September 1985, pp. 1348-1355.
3. Sahu, J. and Chow, W.L.: "A Review of the Fluid Dynamic Aspects of the Effect of Base Bleed", in Base Bleed, K.K. Kuo and J.N. Fleming (Editors), Hemisphere Publishing Corp., NY, 1991, pp. 81-92.
4. Strahle, W.C.: "Base Burning Performance at Mach 3", loc. cit. pp. 217-225.
5. Lanzo, C.D.: "A Flow on a Curved Porous Wall Gas Core Reactor Geometry", NASA TMX-1852, 1969.
6. Johnson, B.V.: "Exploratory Experimental Study of the Effects of Inlet Conditions on the Flow and Containment Characteristics of Coaxial Flows", Rept. H-910091-21 United Aircraft Res. Lab., Sept. 1969.
7. Johnson, B.: "Experimental Study of Multicomponent Coaxial Flow Jets in Short Chambers", NASA CR-1190, 1968.
8. Gurfink, M.M.: "Gas Core Nuclear Thermal Rocket Engine Research and Development in the Former USSR", INEL Report EGG-NE-10391, Sept. 1992.
9. Sforza, PM., Cresci, R.J., and Girlea, F.: "Fuel Efficient Hydrodynamic Containment for Gas Core Fission Reactor Rocket Propulsion", IAF-93-R.1.427, 44th Congress of the International Astronautical Federation, Austria, October 1993.
10. Arzt, J., "Confined Axisymmetric Base Flow with Uniform Injection", M.S. Thesis, Polytechnic University, Brooklyn, NY, January 1996.
11. Sforza, P.M., Cresci, R.J., Arzt, J., and Castrogiovanni, A., "Recirculation Containment for Gas Core Fission Rockets, AIAA Paper 94-2899, AIAA 30th Joint Propulsion Conference, June 1994.
12. Lightman, A.J., and Magill, P.D., "Velocity Measurements in Confined Dual Coaxial Jets Behind an Axisymmetric Bluff Body: Isothermal and Combusting Flows", Univ. of Dayton Research Institute, Report AFWAL-TK-81-2018, April 1981.

13. Porteiro, J.L.F., Przirembel, C.E.G., and Page, R.H., Modification of Subsonic Wakes Using Boundary Layer and Base Mass Transfer", AIAA Jl, Vol. 21, No. 5, May 1981.

14. Dutton, J.L., et al, "Recent Progress on High Speed Separated Base Flows", AIAA Paper 95-0472, AIAA Aerospace Sciences Meeting, January 1995.

15. Cline, M.C., "VNAP2: A Computer Program for Computation of Two-Dimensional, Time Dependent, Compressible, Turbulent Flow", Los Alamos National lab., Report LA-8872, August 1984.

16. Nietubicz, C.J., and Sahu, J., "Navier-Stokes Computations of Base Bleed Projectiles" in Base Bleed, Ed. by Kuo, K.K., and Fleming, J.N., Hemisphere Publishing 1991.

17. Herrin, J.L. and Dutton, J.C., "Supersonic Base Flow Experiments in the Near Wake of a Cylindrical Afterbody", AIAA Jl, Vol. 32, No. 1, January 1994, pp. 77-83.

18. Scott, J.N. and Hankey, W.L., Jr., "Numerical simulation of Cold Flow in an Axisymmetric Centerbody combustor", AIAA Jl, Vol. 23, May 1985, pp. 641-649.

19. Krishnamurthy, L., "Isothermal Flowfield Predictions of Confined Coflowing Turbulent Jets in an Axisymmetric Bluff-Body Near Wake", AFWAL-TR-81, 2036.

20. Raju, M.S., Creed, M.J., and Krishnamurthy, L., "Comment on Numerical Simulation of Cold Flow in an Axisymmetric Centerbody Combustor", AIAA Jl, Vol. 24, No. 4., April 1986, pp. 698-701.

21. Lee, S.W., "Centerline Velocity Measurements in Axisymmetric Base Flows", M.S. Thesis, Polytechnic University, Brooklyn, NY, June 1997.

Appendix A

Polytechnic University's Gas Dynamics Facility

Introduction

The Preston R. Bassett Research Laboratory houses the Aerodynamics Laboratory facilities of the Aerospace Engineering Department and is located at Polytechnic's Long Island Center. The research center was constructed with the support of NASA. It is composed of offices for staff and students, a computer room, administrative offices, instrumentation laboratories, machine shop, and wind tunnels and associated equipment. The Gas Dynamics Research Facility consists of an air supply and storage system, various supersonic and hypersonic tunnels, vacuum pumping equipment used to exhaust the tunnels, and a vacuum sphere.

The Air Supply and Storage System

Two Worthington four-stage compressors are available to pressurize the air to approximately 170atm (2500 psia) at a pumping rate of 0.5kg (0.25 pounds) of air per second per compressor. The high pressure air leaves the compressors and flows through a system of separators which remove the oil and water vapor from the gas, and then through a system of silica gel driers which dry the air to a dew point below 233K (-40F). From the driers, the gas flows into the high rpessure storage flasks and is available for utilization in the various tunnels. These flasks are manifolded into two banks of 25 tanks each; they are designed to operate at a pressure fo 300 atm (4500 psia) although they are not6 pressurized above 170 atm (2500 psia) for the present testing purposes. Each of the two banks has a volume of 28 cubic meters (1000 cubic feet) and can be put on the line either individually or jointly. The main supply line feeding the tunnels is connected by valves to the supersonic settling chamber, the heater for the hypersonic tunnels, and an additional smalljet which can be used for subsonic mixing tests or for other types of facilities requiring low mass flow.

Appendix B

Publications Related to Present Project

Reports generated with the support of the present project, including efforts expended after the official termination of the grant have been cited in the body of this report as Refs. 9, 11, 10, and 21. They are listed again here for convenience:

Sforza, P.M., Cresci, R.J., and Girlea, F., "Fuel Efficient Hydrodynamic Containment for Gas Core Fission Reactor Rocket Propulsion", IAF-93-R.1.427, 44th Congress of the International Astronautical Federation, October, 1993.

Sforza, P.M., Cresci, R.J, Arzt, J., and Castrogiovanni, A., "Recirculation Containment for Gas Core Fission Rockets", AIAA 94-2899, AIAA 30th Joint Propulsion Conference, June 1994.

Arzt, J., "Confined Axisymmetric Base Flow with Uniform Injection", M.S. Thesis, Polytechnic University, Brooklyn, NY, January 1996.

Lee, S., "Centerline Velocity Measurements in Axisymmetric Base Flows", M.S. Thesis, Polytechnic University, Brooklyn, NY, June 1997.

Table 1

Full Scale Reactor Characteristics According to Gurfink [Ref. 6]

Containment region pressure	350 - 1000 atm
Propellant velocity	100-1500 fps
Propellant density	0.1 - 0.5 lbm/ft^3
Uranium density	0.6 - 0.9 lbm/ft^3
Fuel containment diameter	2.6 - 3.6 ft
Annular propellant width	0.25 - 0.5 ft
Cavity length	3.3 - 5 ft
Density ratio (fuel/propellant)	2 - 6
Reynolds number (propellent)	10^5 to 10^7

Table 2

Summary of Test Model Characteristics:

OD = 16.0" (outside diameter)	$Re = 5.75 \times 10^5$
ID = 15.25" (test section diameter)	$w_a = 50$ ft/s
D = 10.75: (base diameter)	m = 4.86 lbm/s
d = 2.25" (annulus height)	$P_0 = 2$ atm
D^* = 3.0" (throat diameter)	$T_0 = 535^oR$

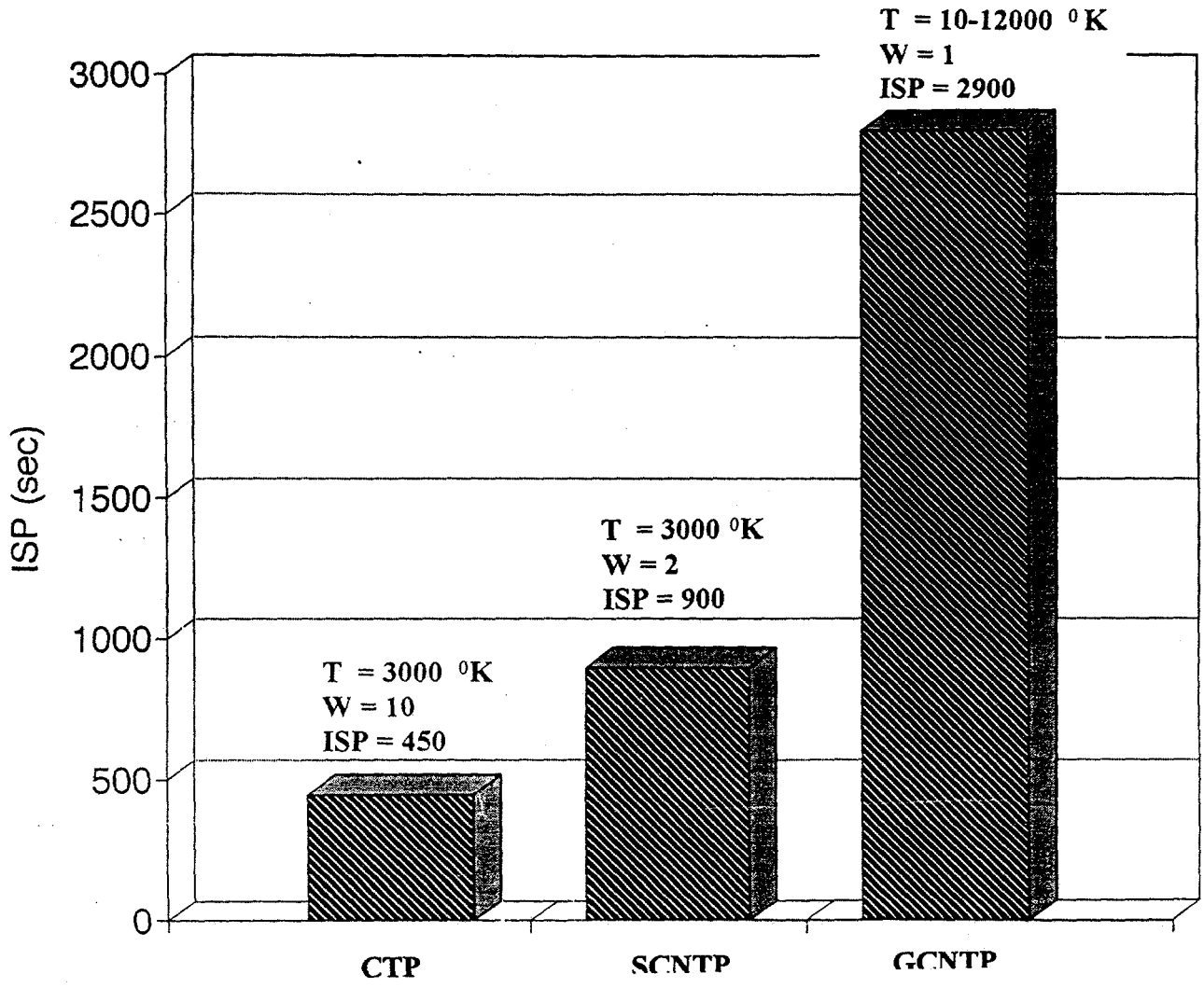

Fig. 1 Comparison of specific impulse for various rocket systems

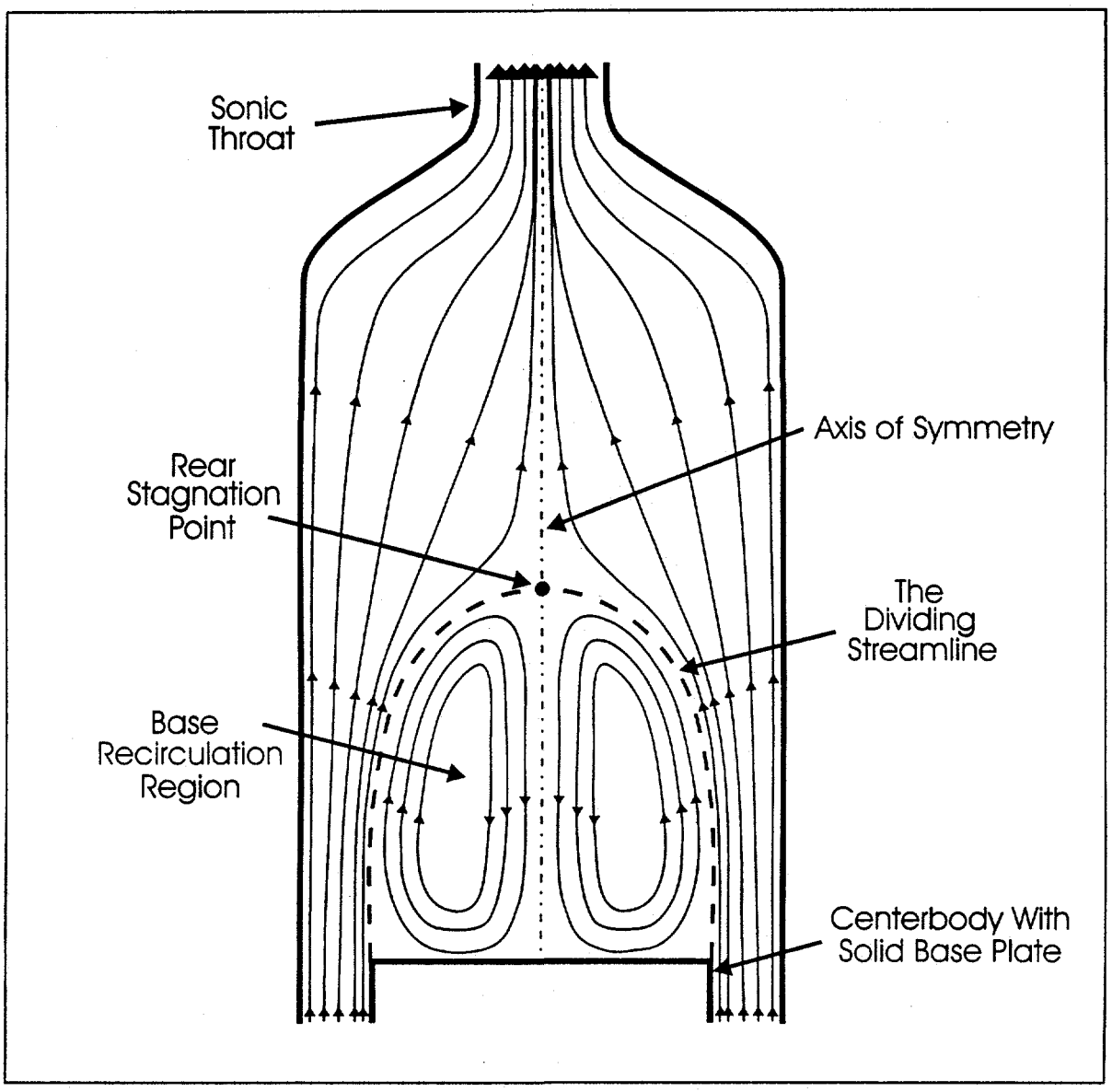

Fig. 2 Flow without base bleed injection into the recirculation region

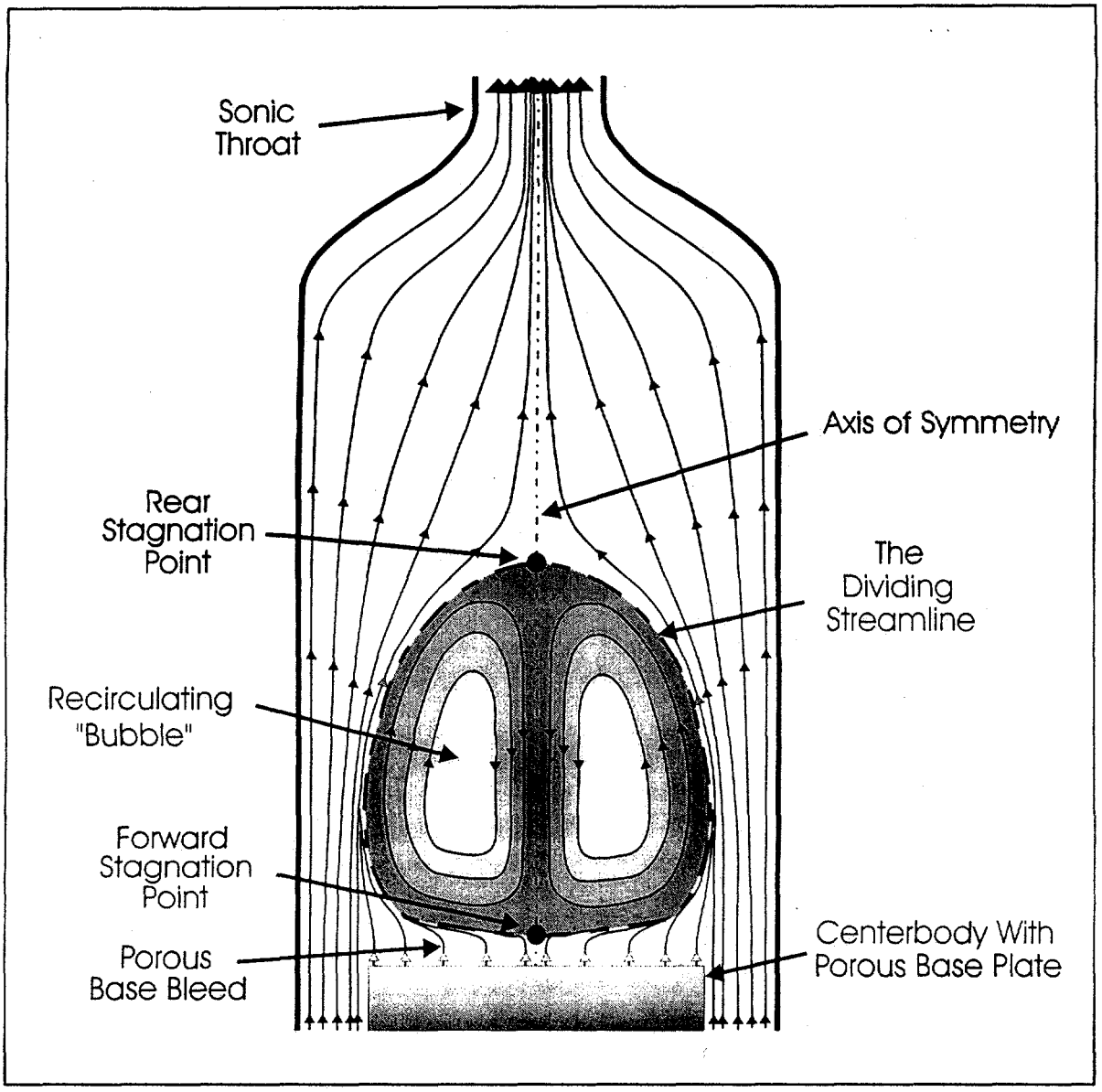

Fig. 3 **Flow with porous base bleed showing detached recirculation bubble**

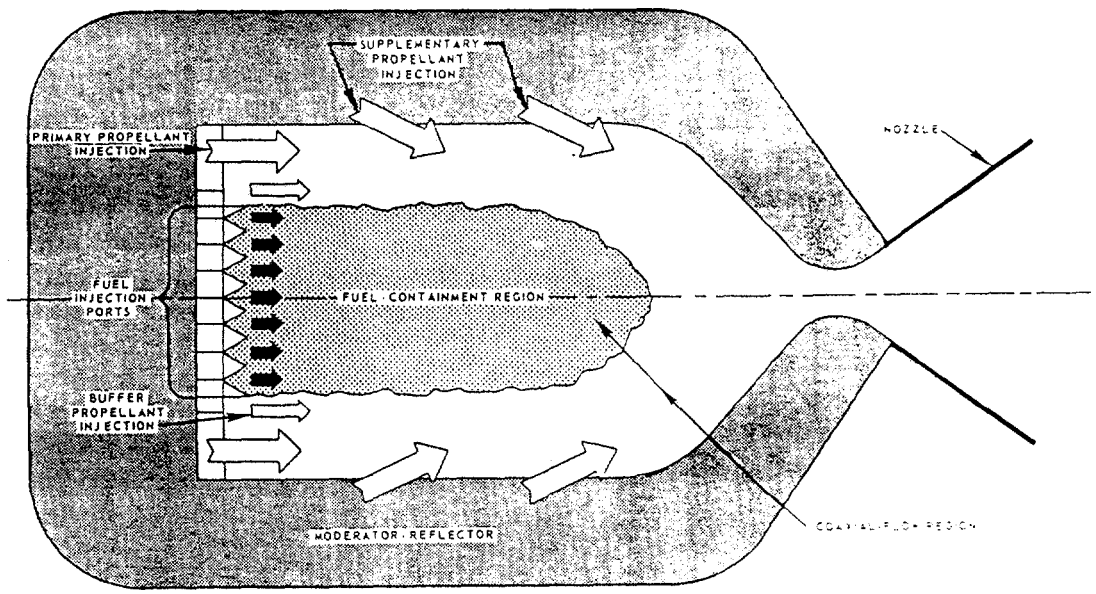

Fig. 4 Schematic of a gas core nuclear rocket - Ref. [7]

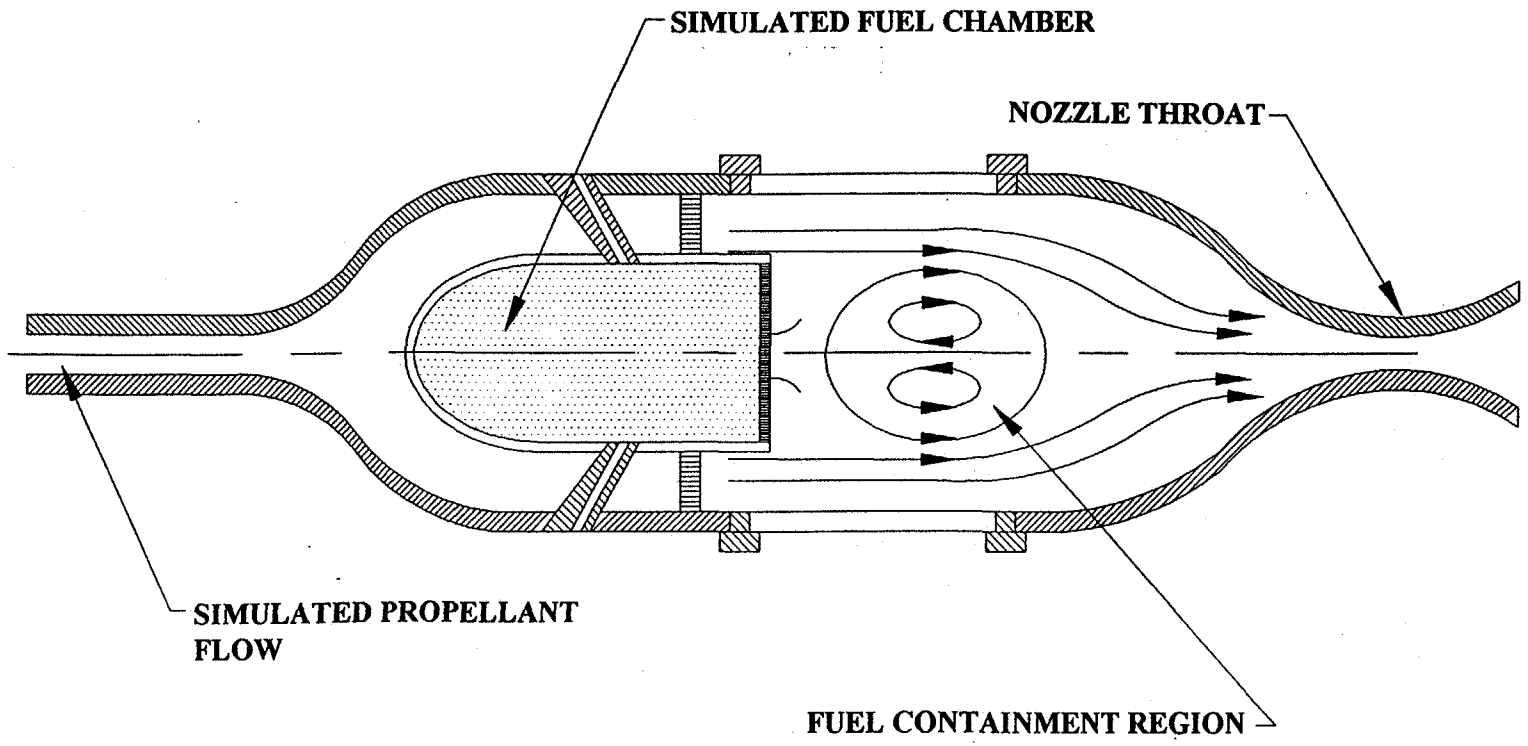

Fig. 5 Schematic of flow simulation system

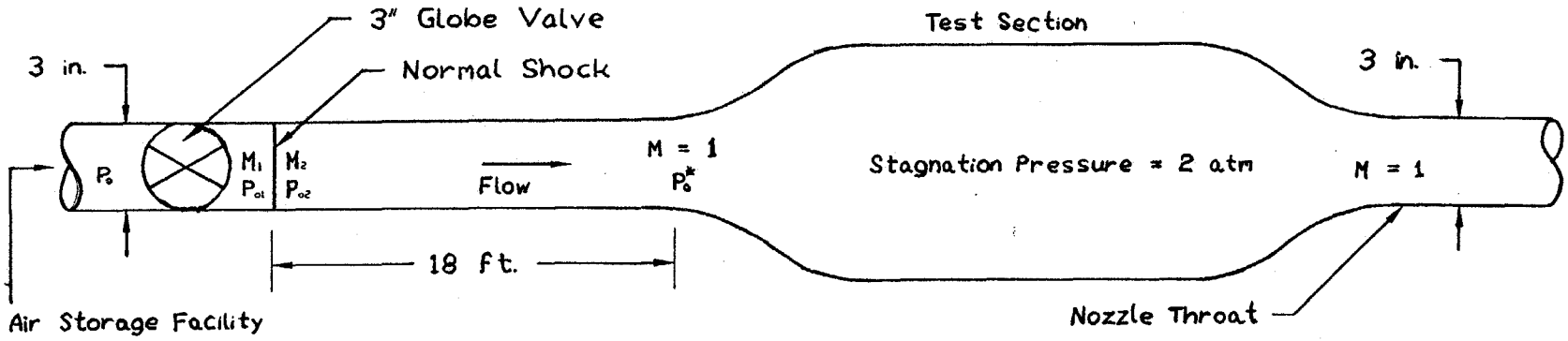

Fig. 6 Schematic of Fanno line problem

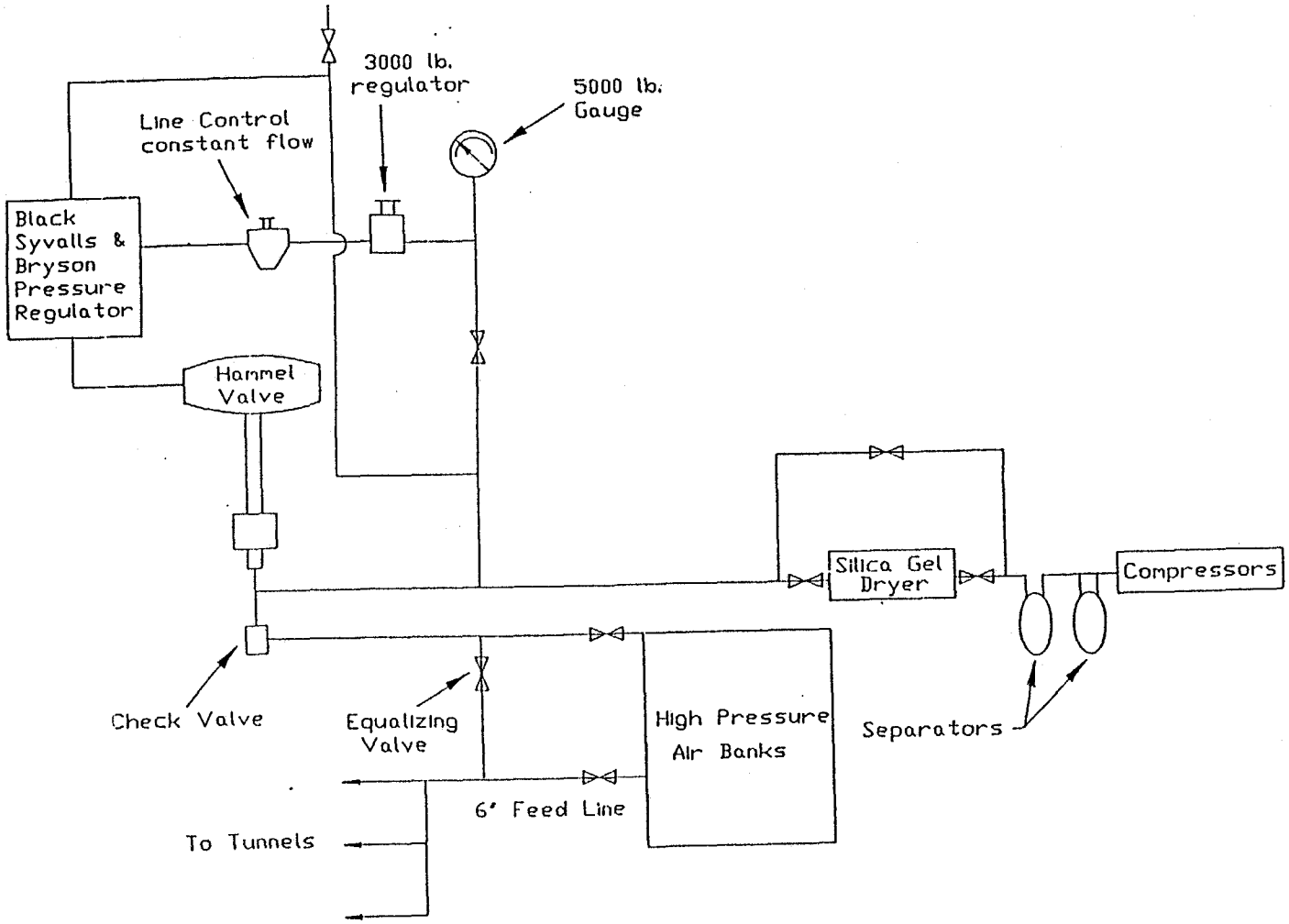

Fig. 7 Polytechnic University air supply system

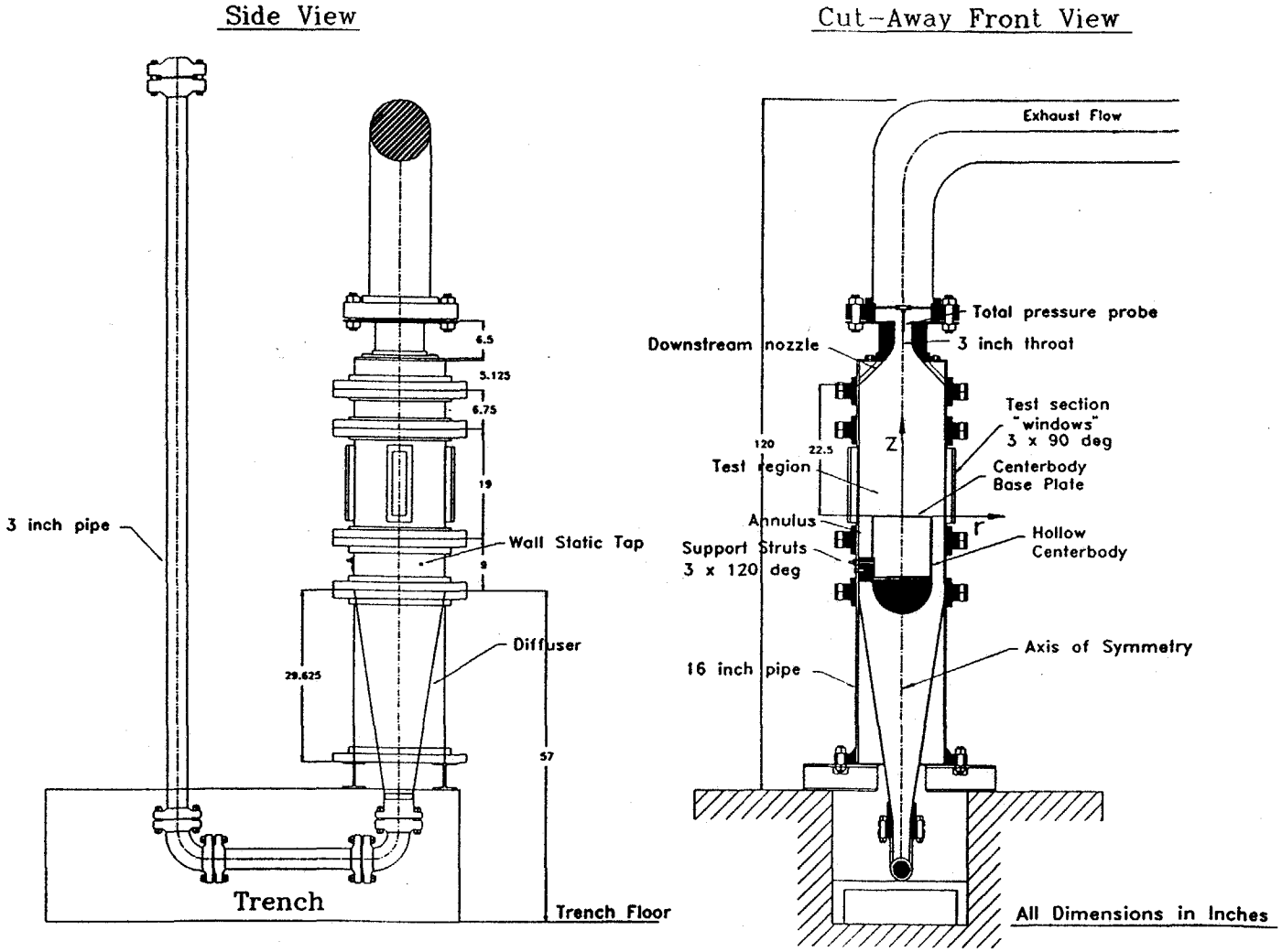

Fig. 8 Overall diagram of original test facility

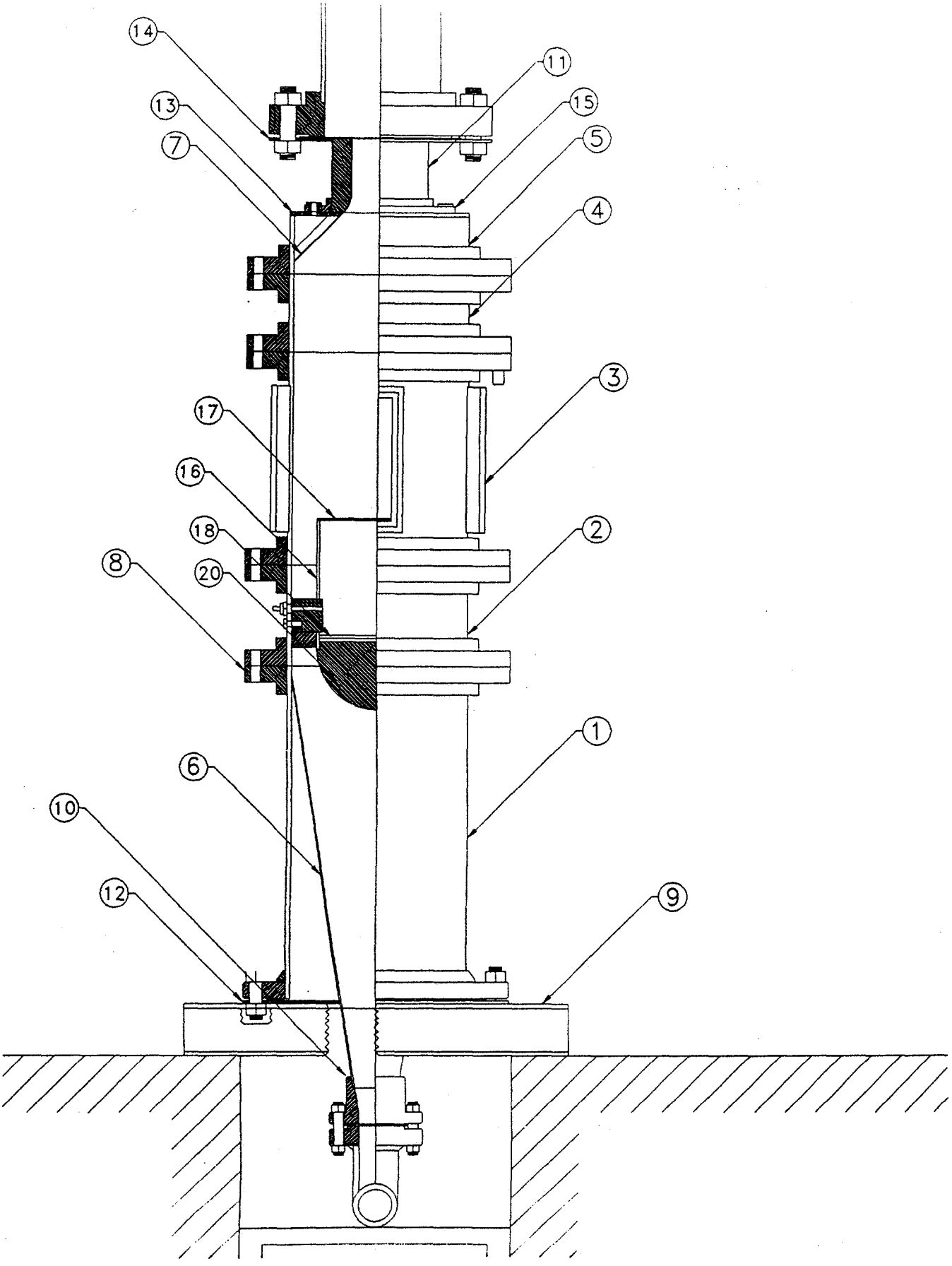

Fig. 9 Assembly drawing of original test facility

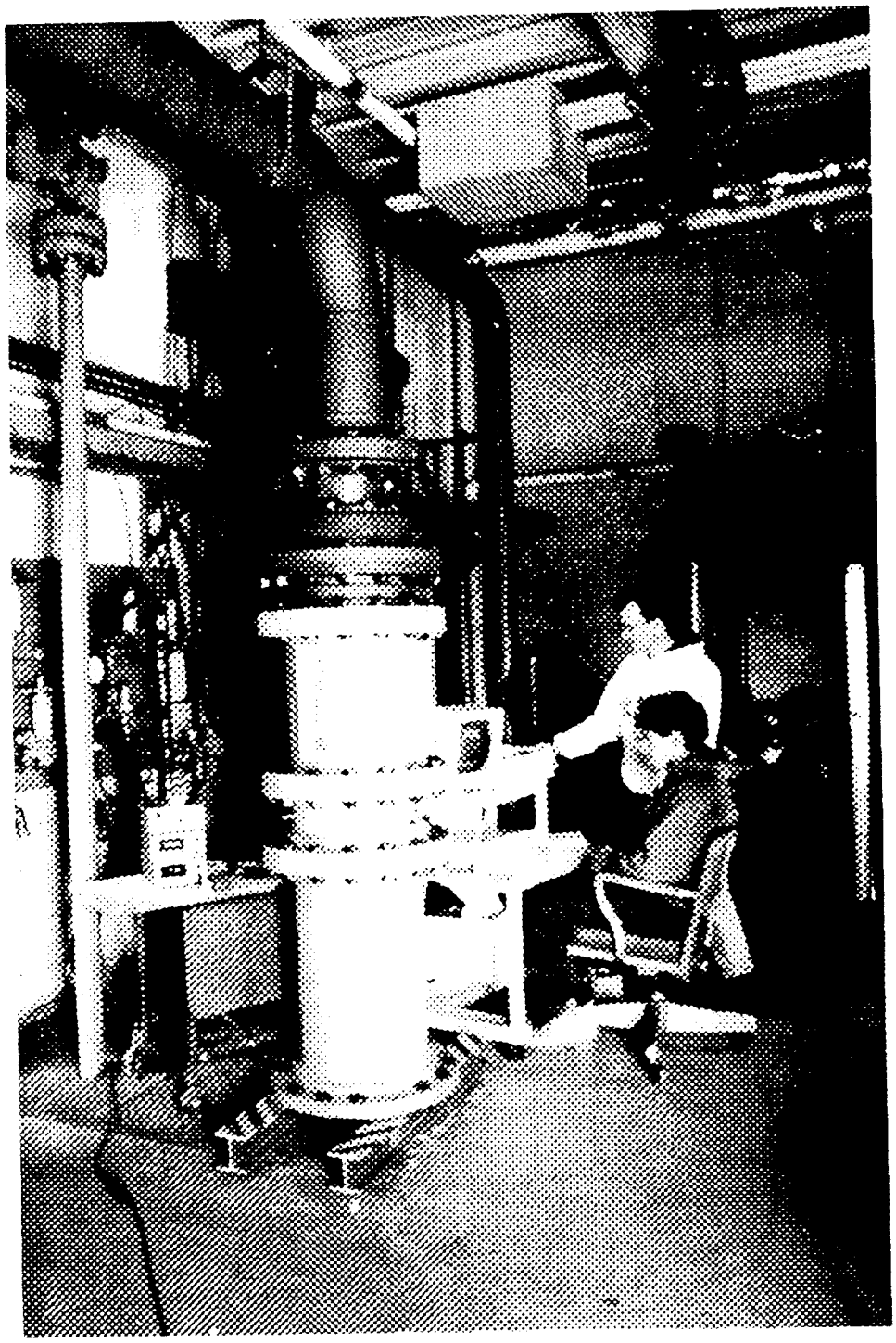

Fig. 10 Photograph of the original test facility

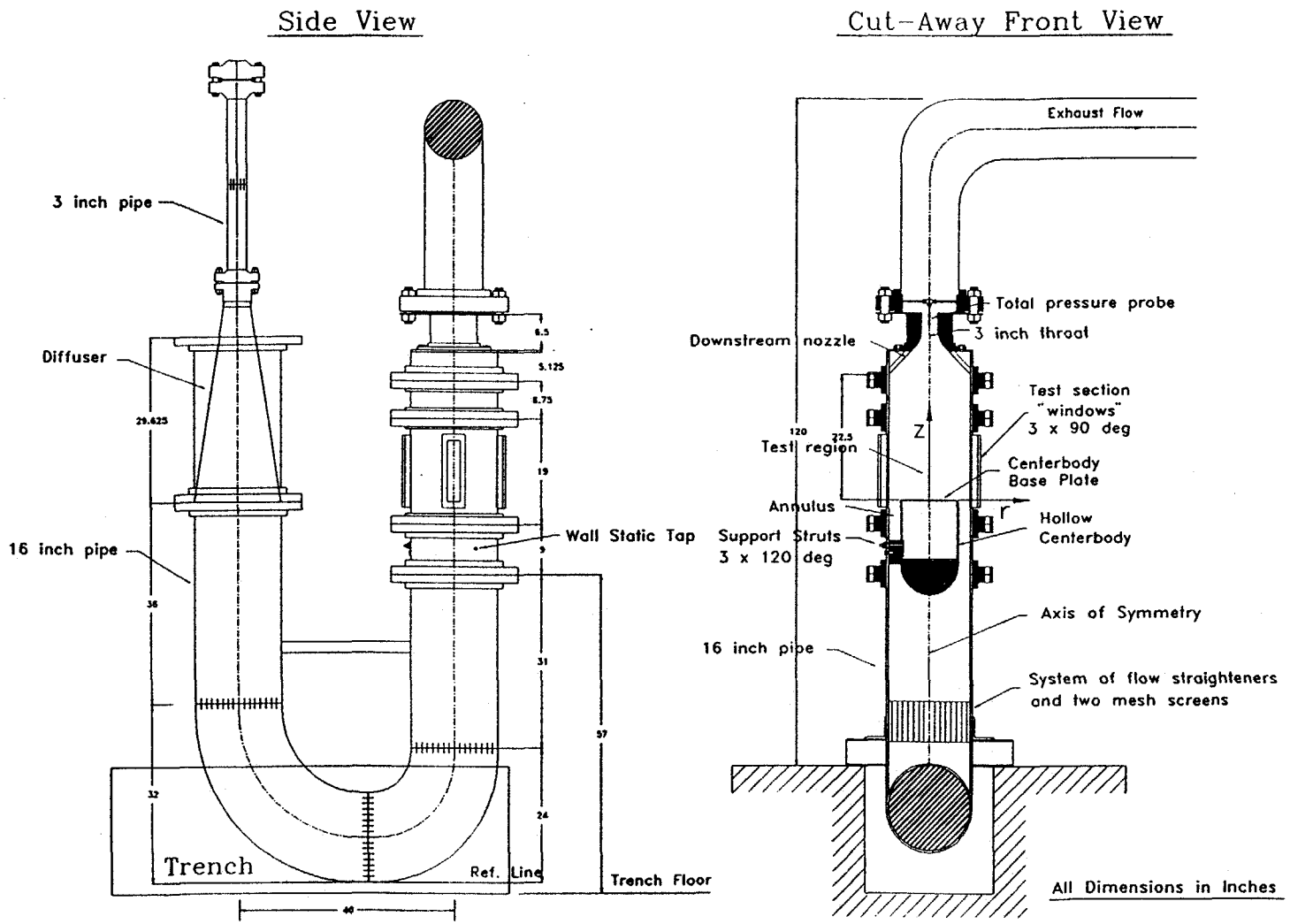

Fig. 11 Schematic diagram of improved test facility

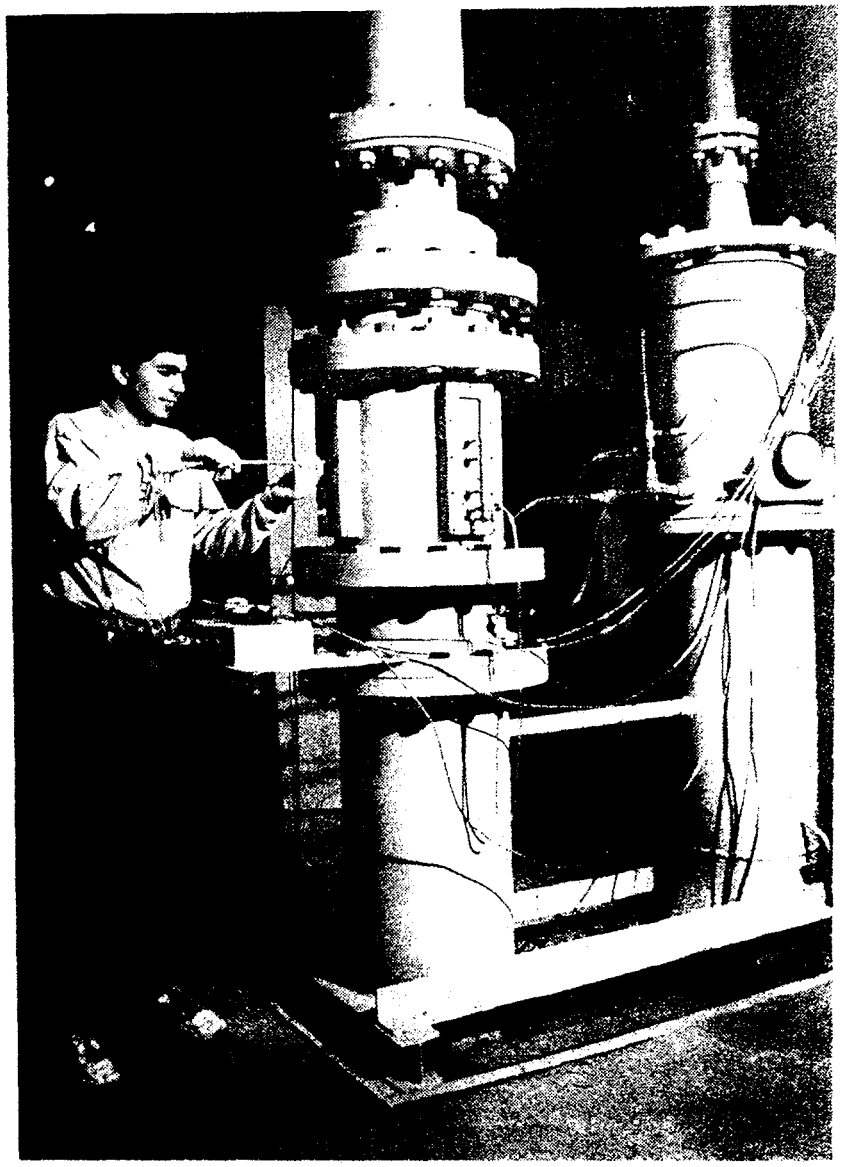

Fig. 12 Photograph of the improved test facility

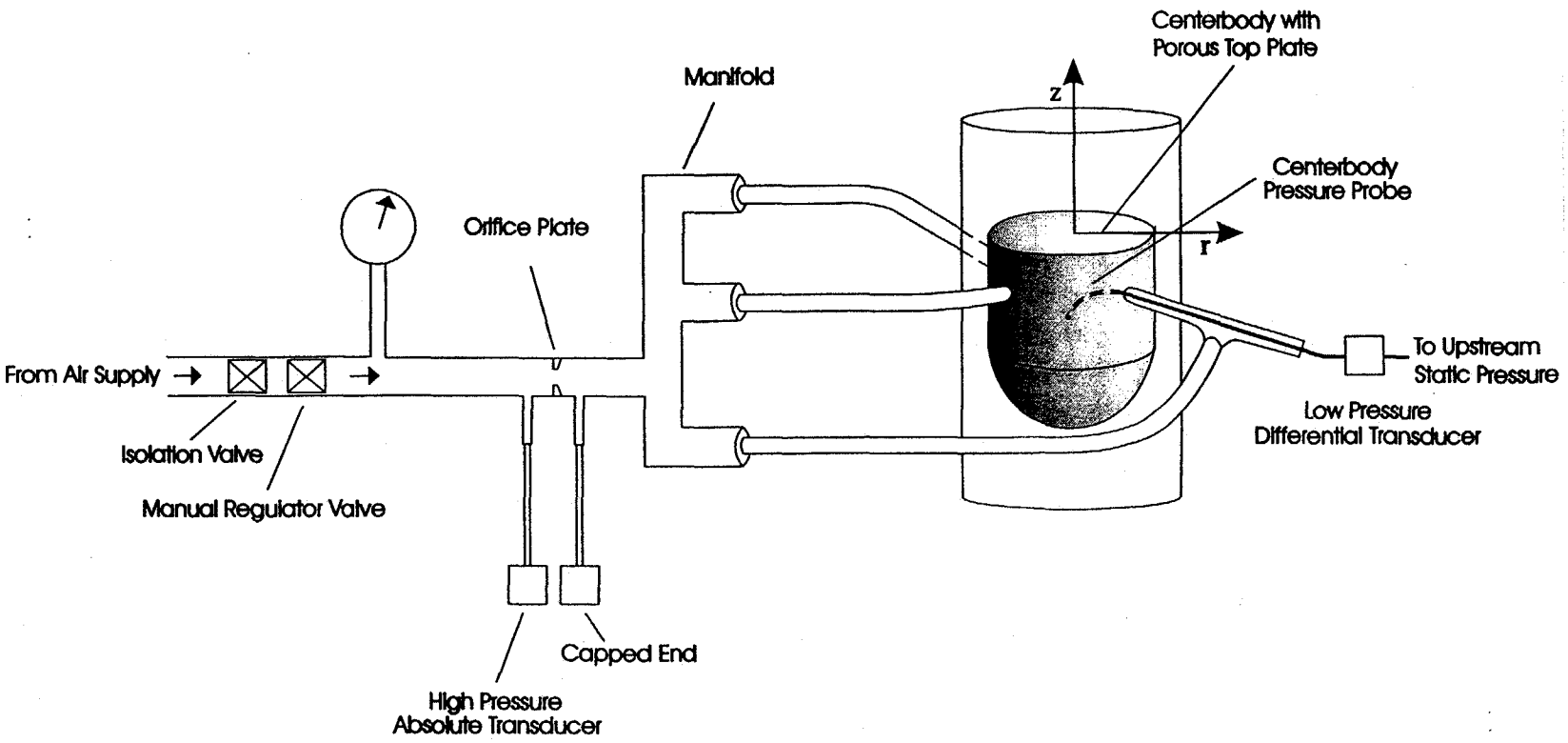

Fig. 13 Schematic diagram of the porous base plate injection system

Fig. 14 Photograph of the pitot rake positioned over the annulus

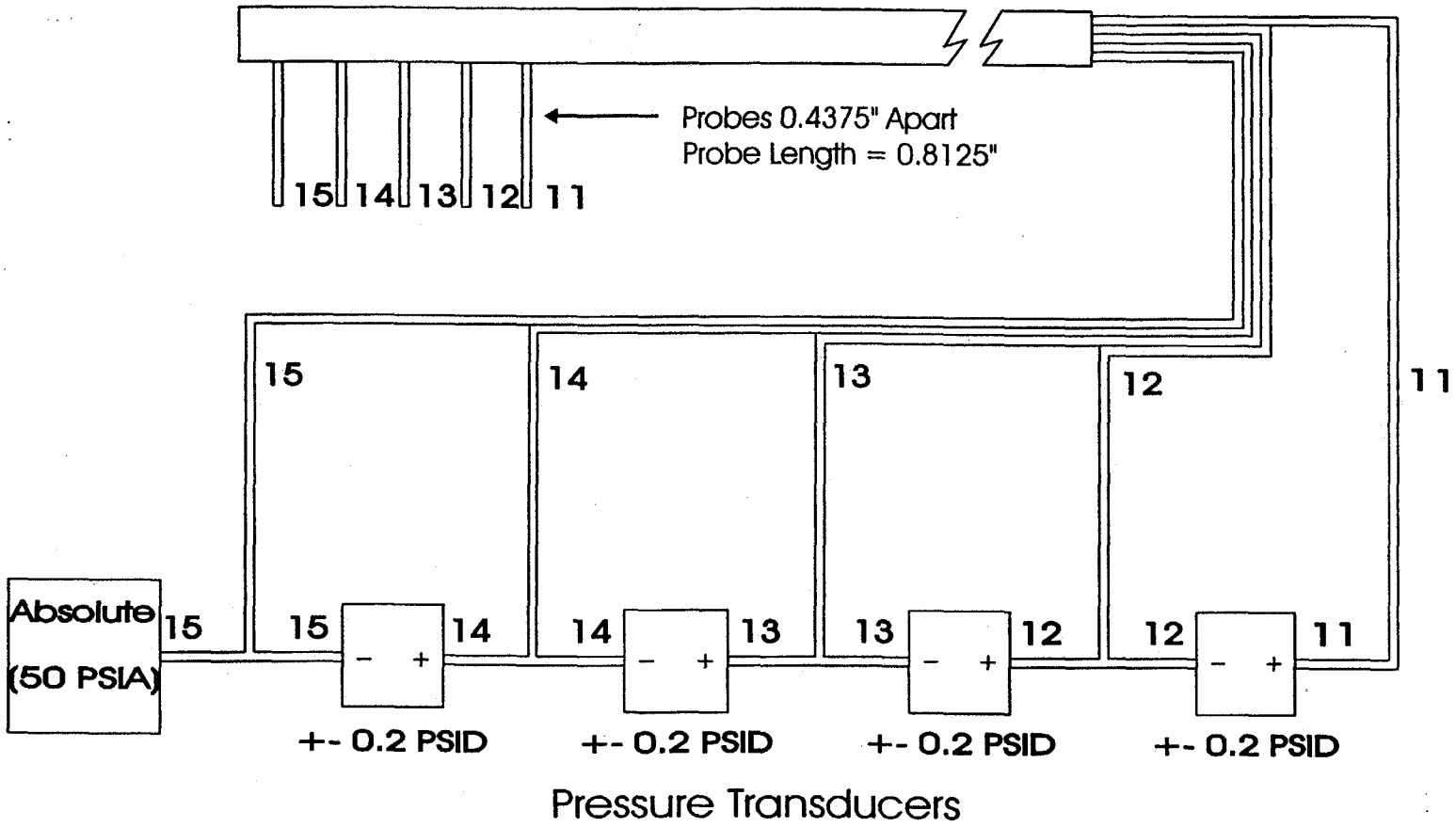

Fig. 15 Schematic diagram of the rake instrumentation set-up

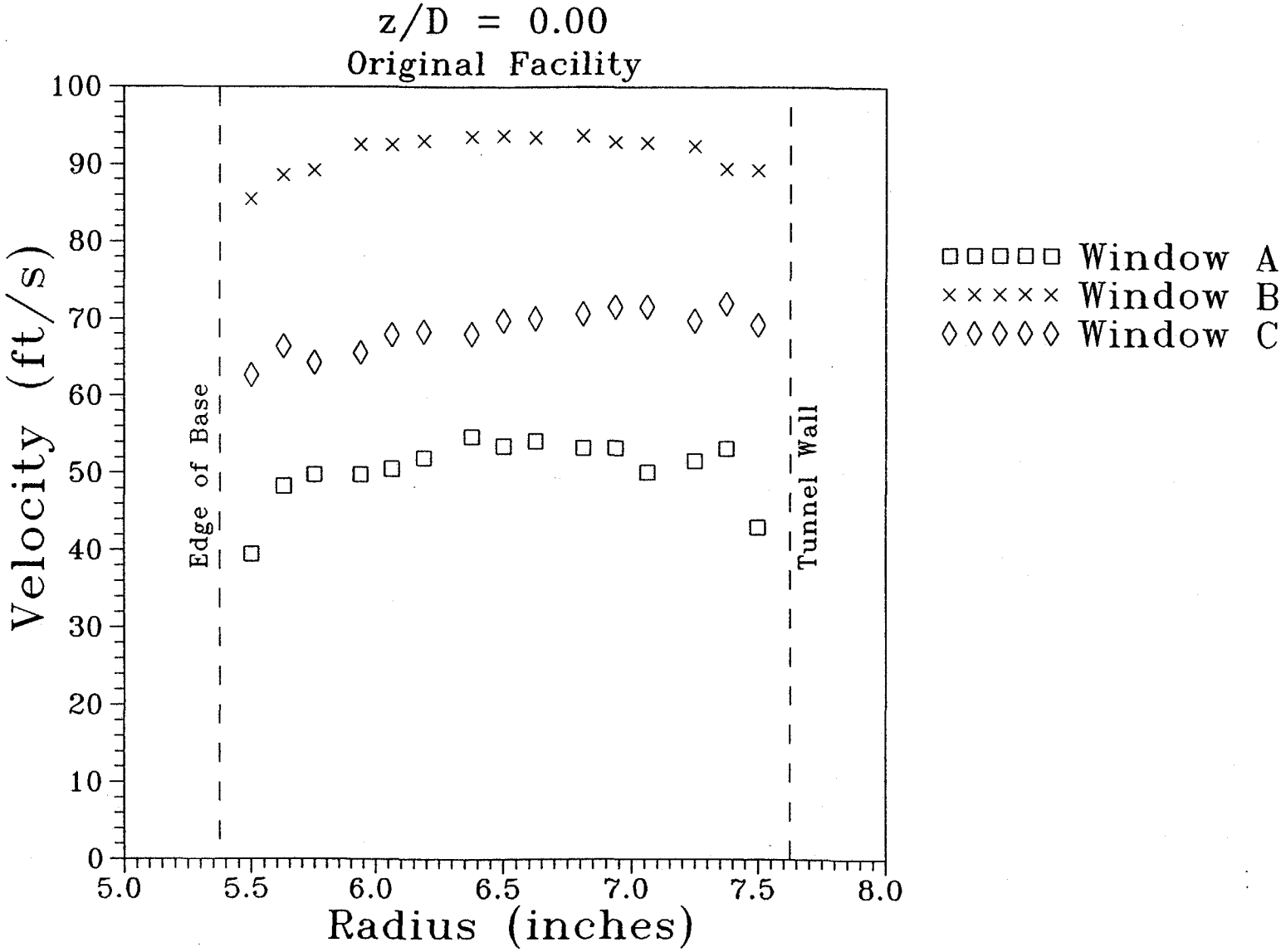

Fig. 16 Velocity as a function of radius in the annulus at the plane of the base, z/D = 0, in the original test facility

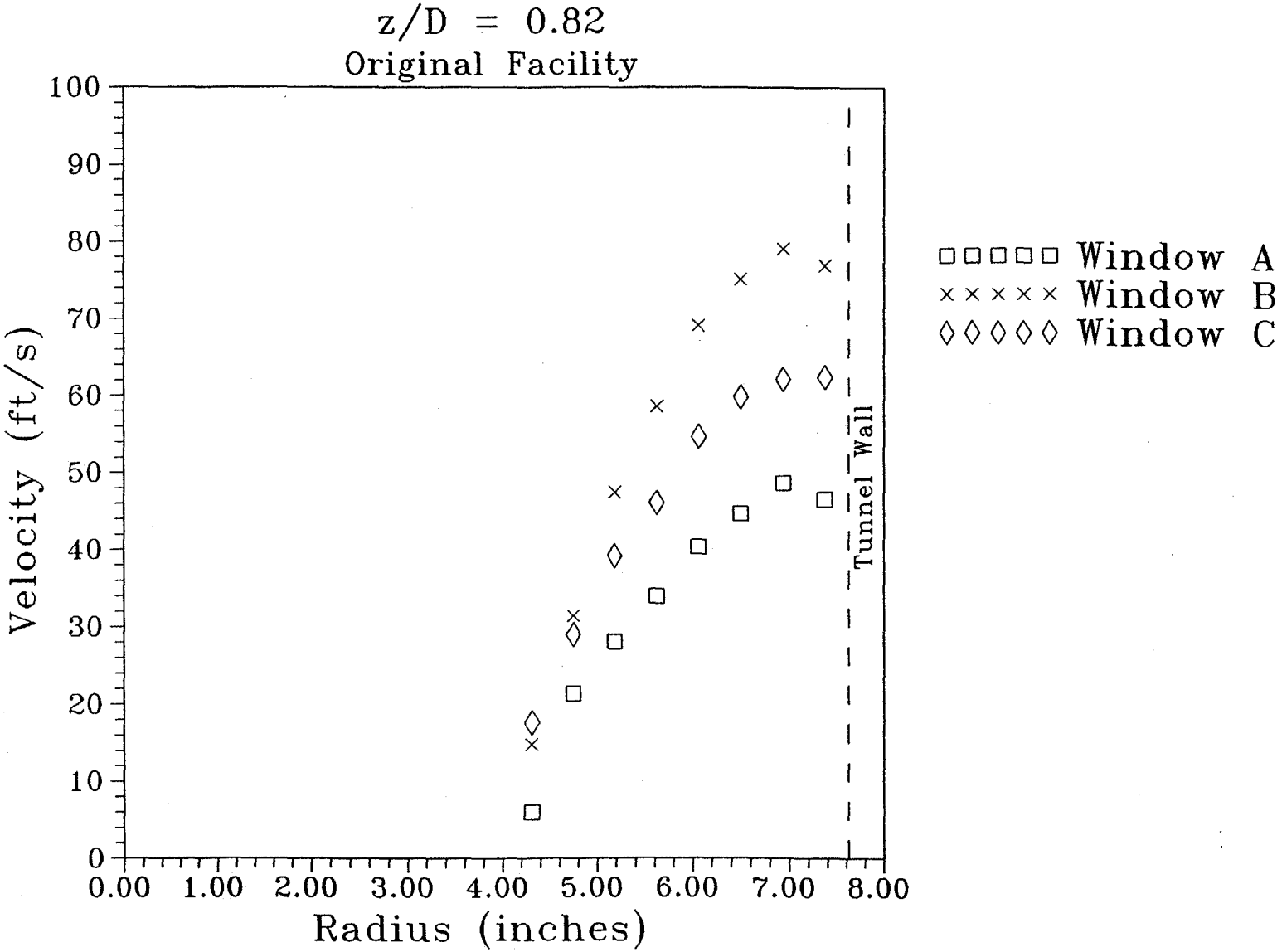

Fig. 17 Velocity as a function of radius for the axial location z/D = 0.82 in the original test facility

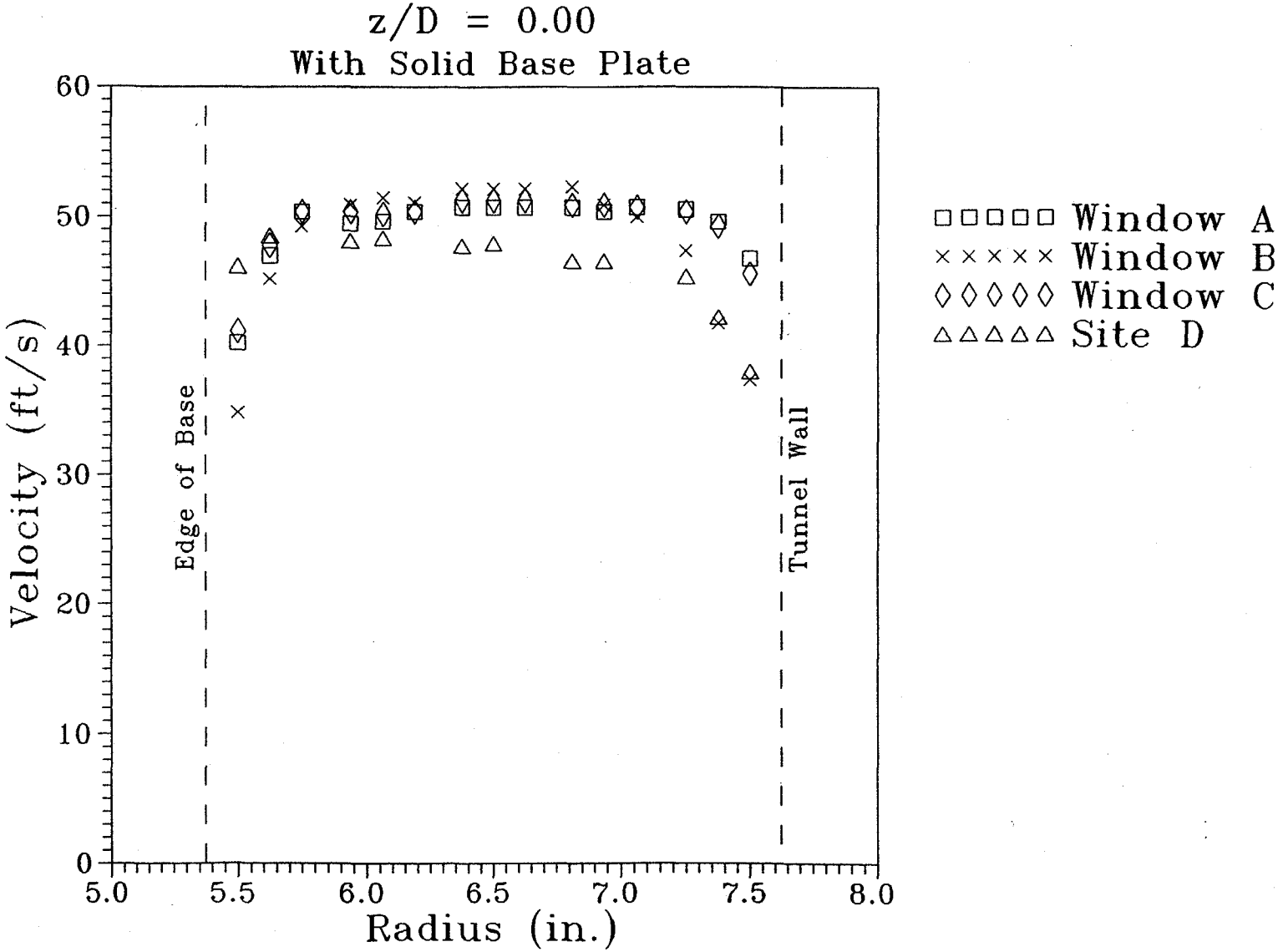

Fig. 18 Velocity as a function of radius in the annulus at the plane of the base, z/D = 0, in the improved test facility

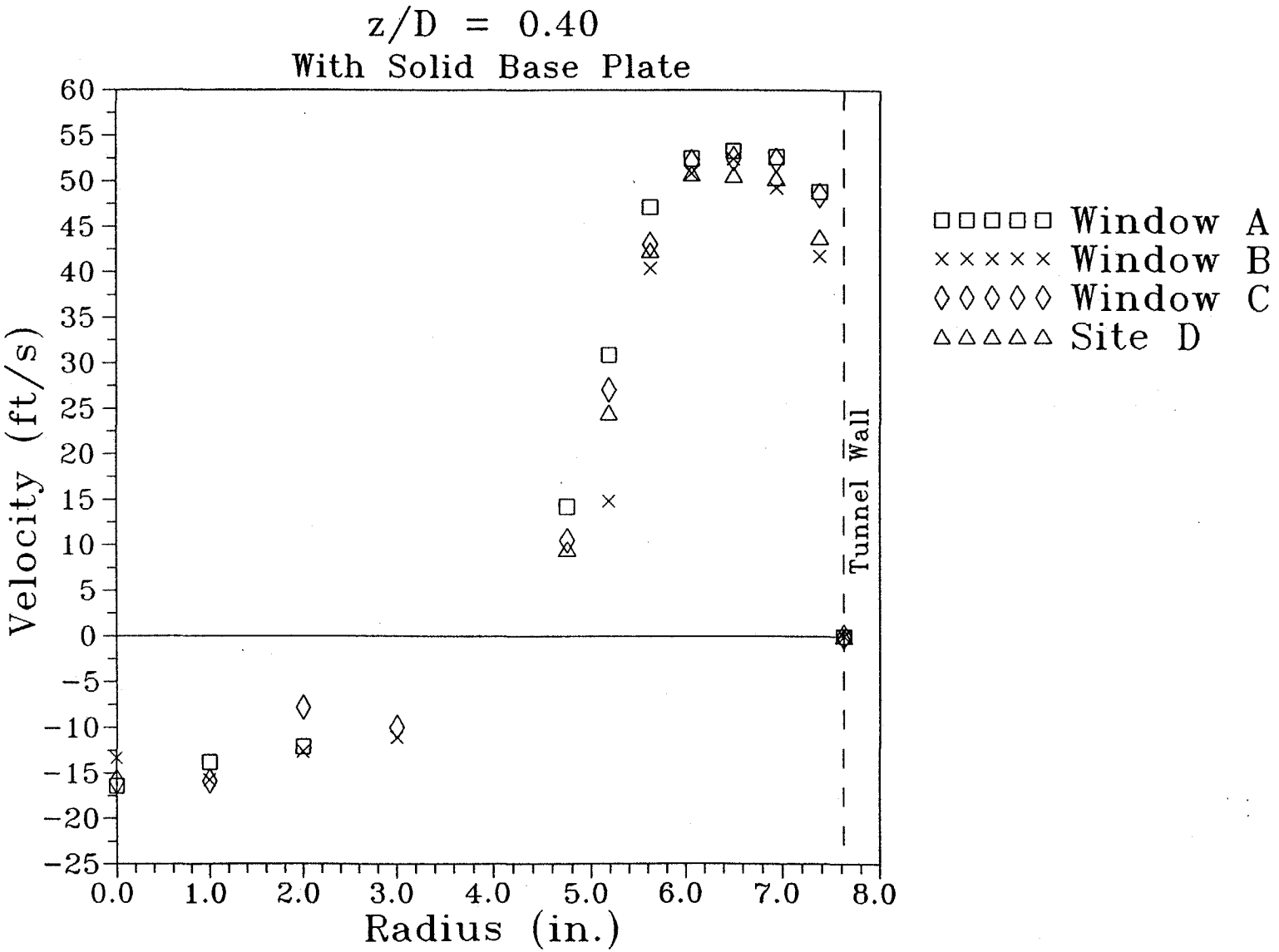

Fig. 19 Velocity as a function of radius for the axial location z = 0.40 in the improved test facility

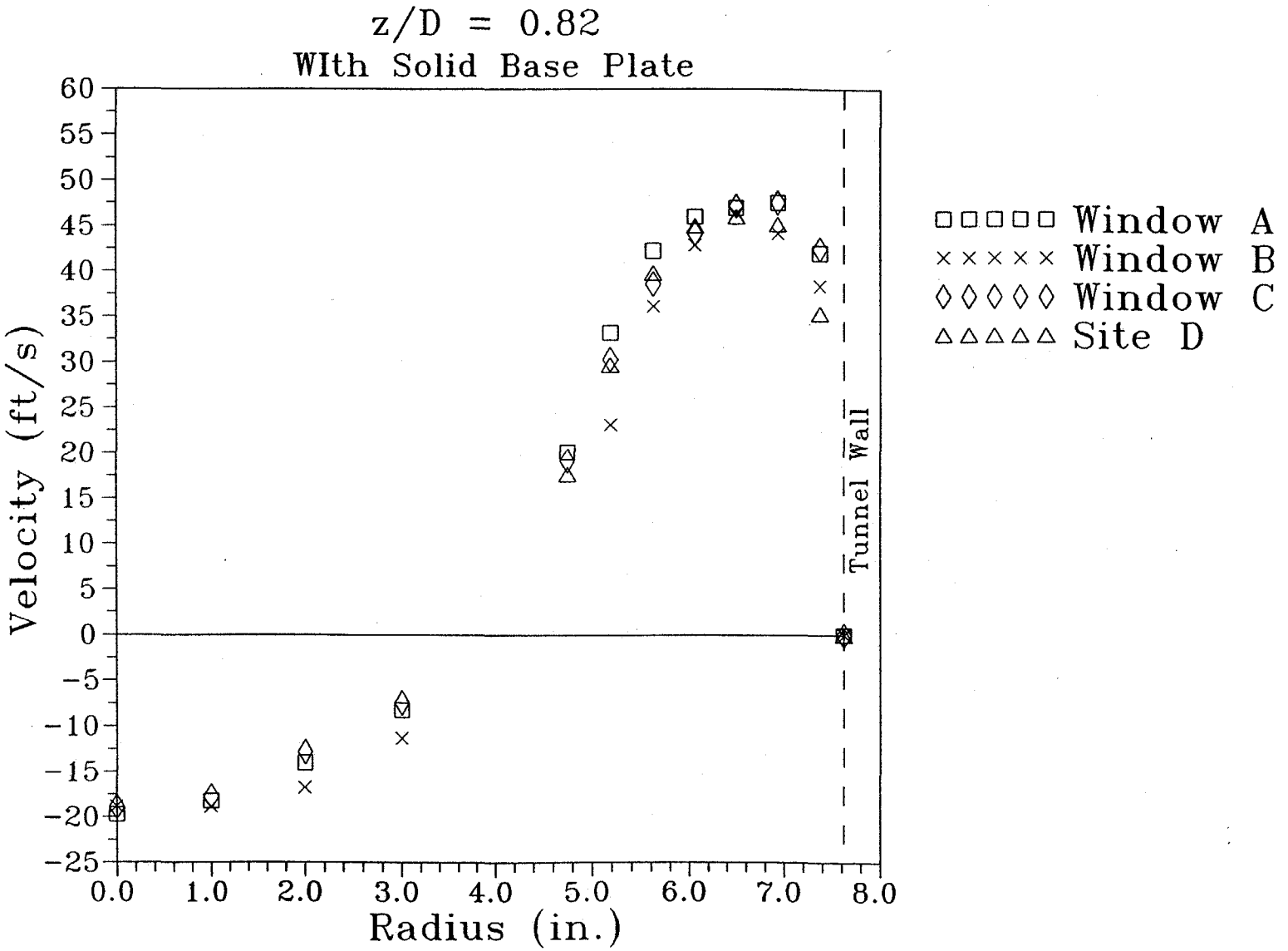

Fig. 20 Velocity as a function of radius for the axial location z = 0.82 in the improved test facility

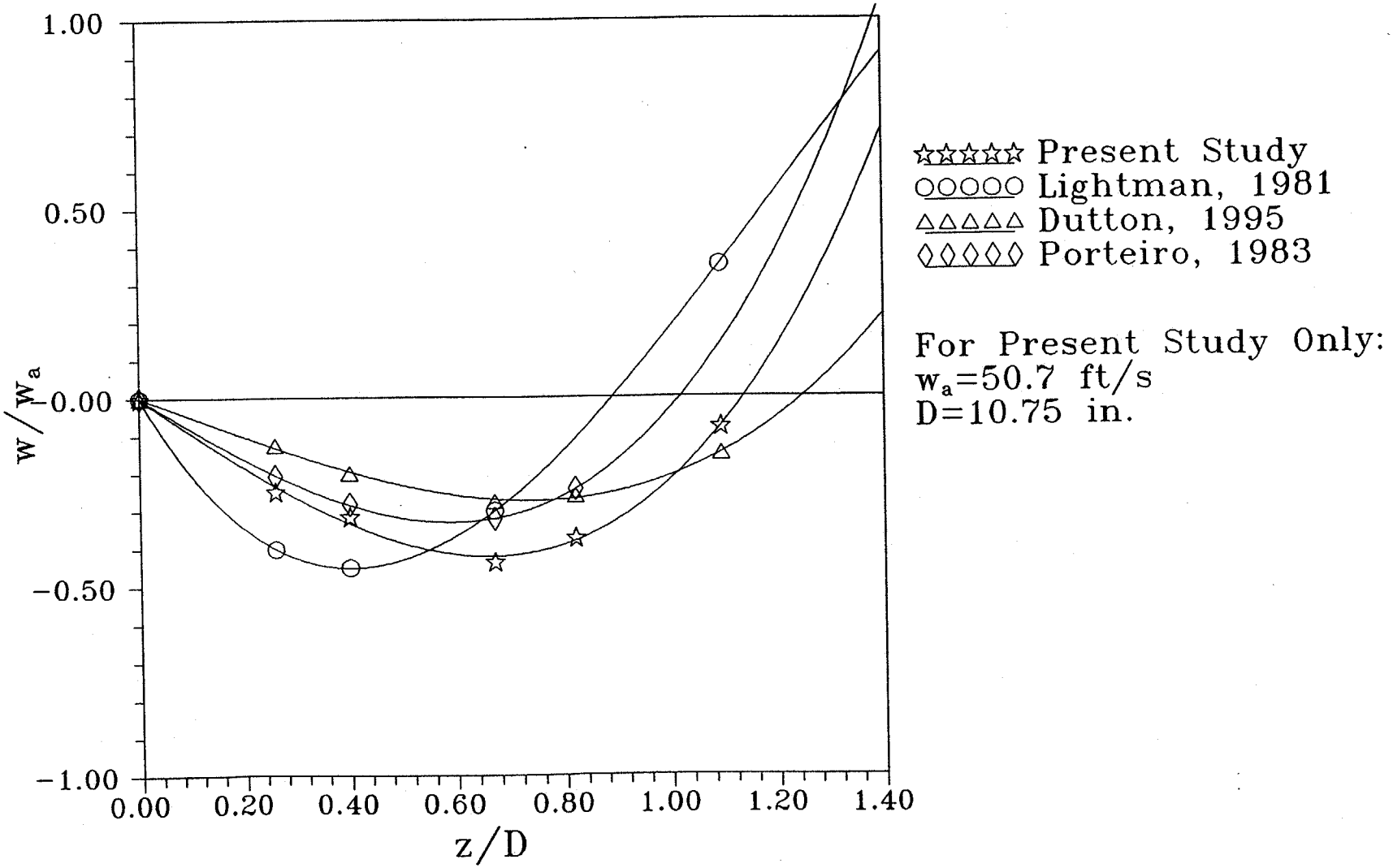

Fig. 21 Centerline velocity ratio w/w_a as a function of z/D for zero injection

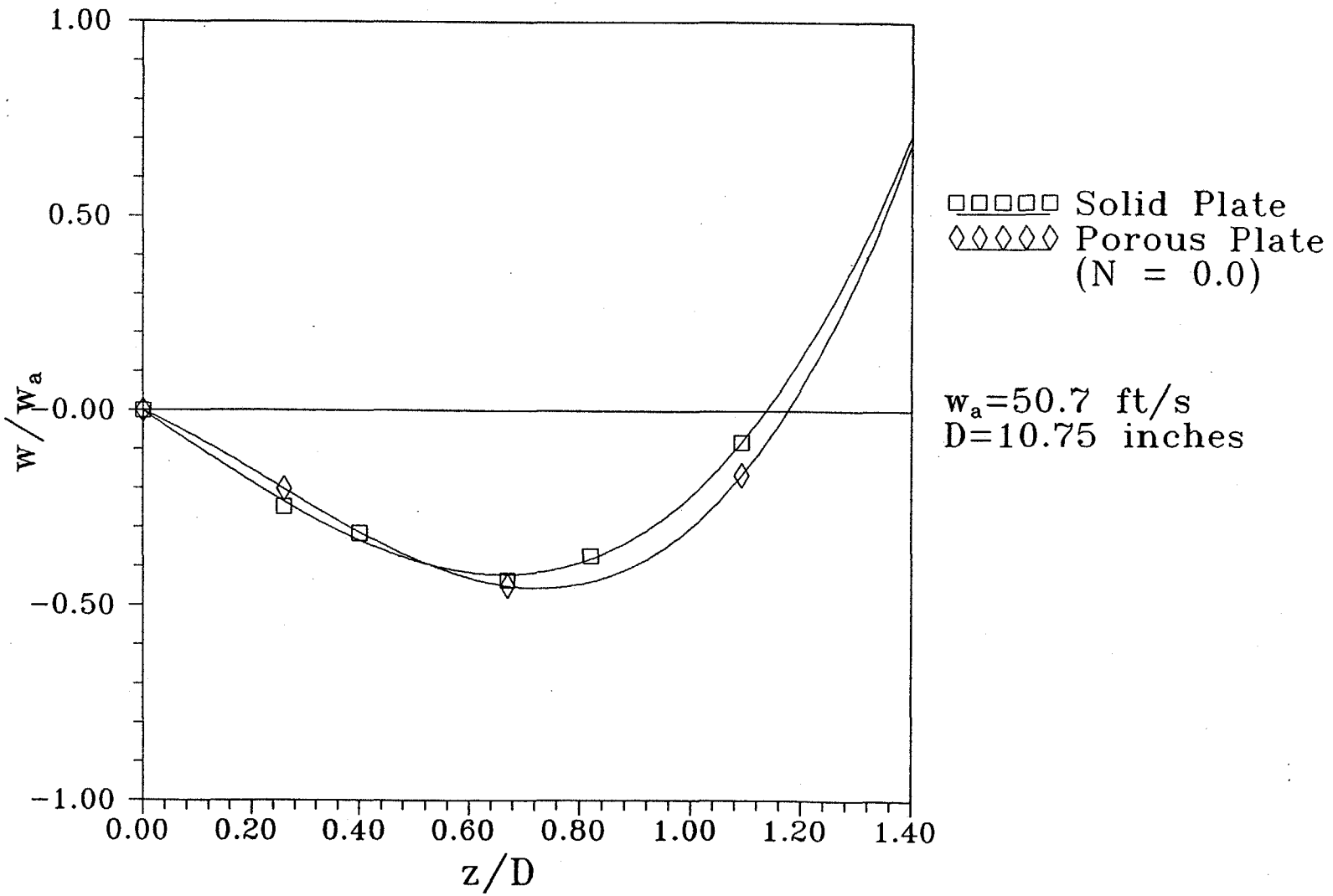

Fig. 22 Centerline velocity ratio w/w_a as a function of z/D for zero injection for the solid and the porous base cases

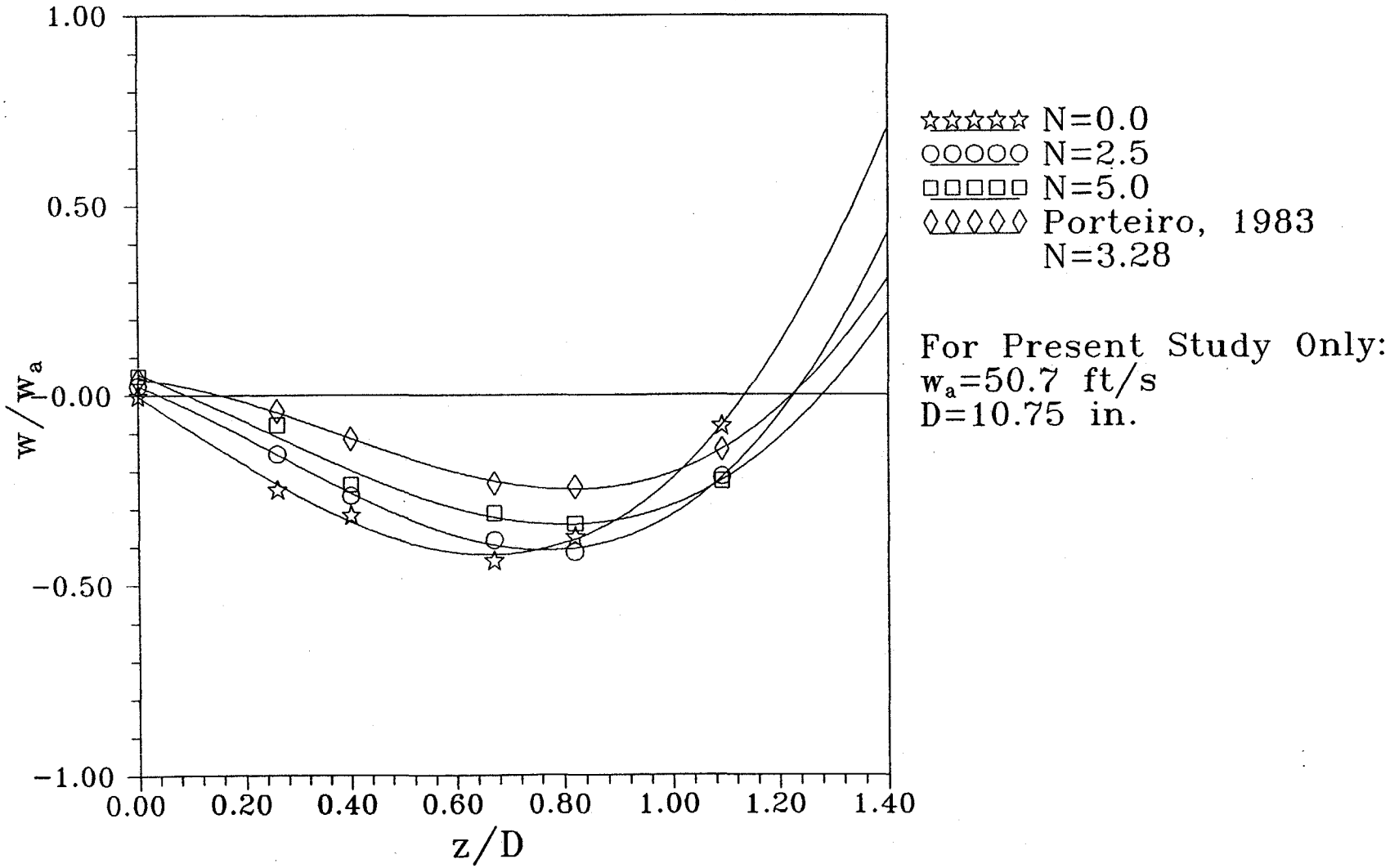

Fig. 23 Centerline velocity ratio w/w_a as a function of z/D for various values of the base bleed ratio N

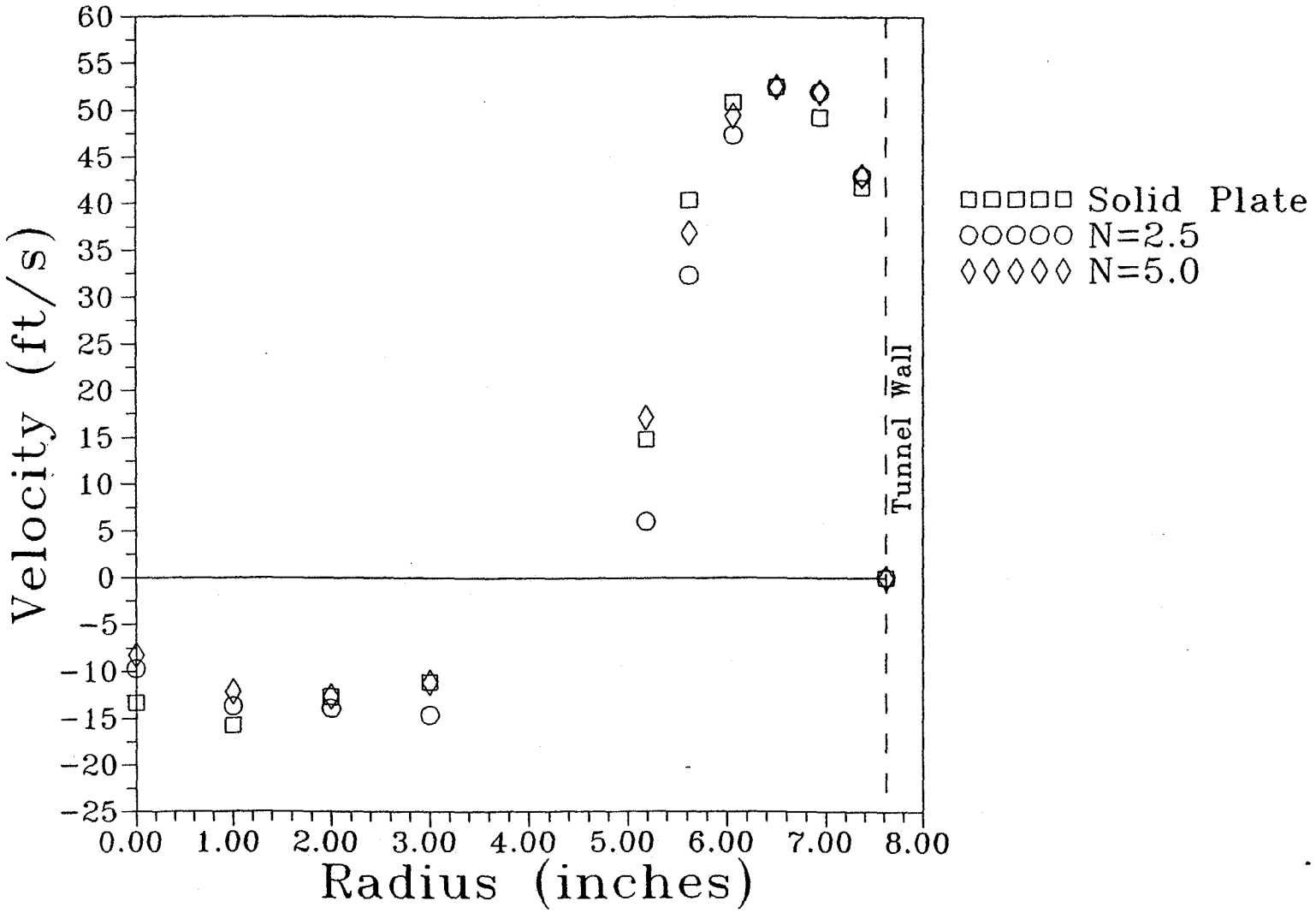

Fig. 24 Velocity as a function of radius for z/D = 0.40 at window B for various values of the base bleed ratio N

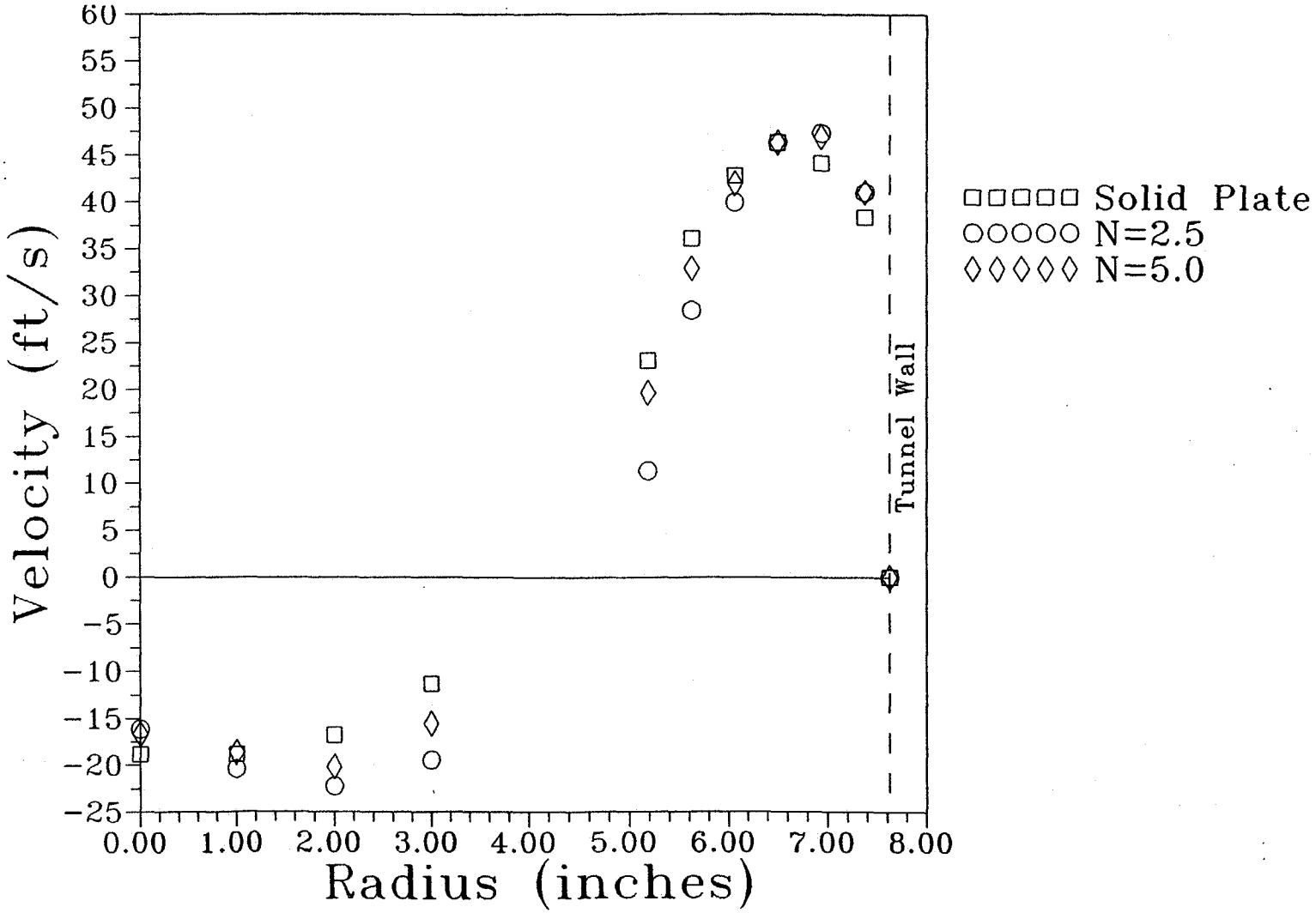

Fig. 25 Velocity as a function of radius for z/D = 0.82 at window B for various values of the base bleed ratio N

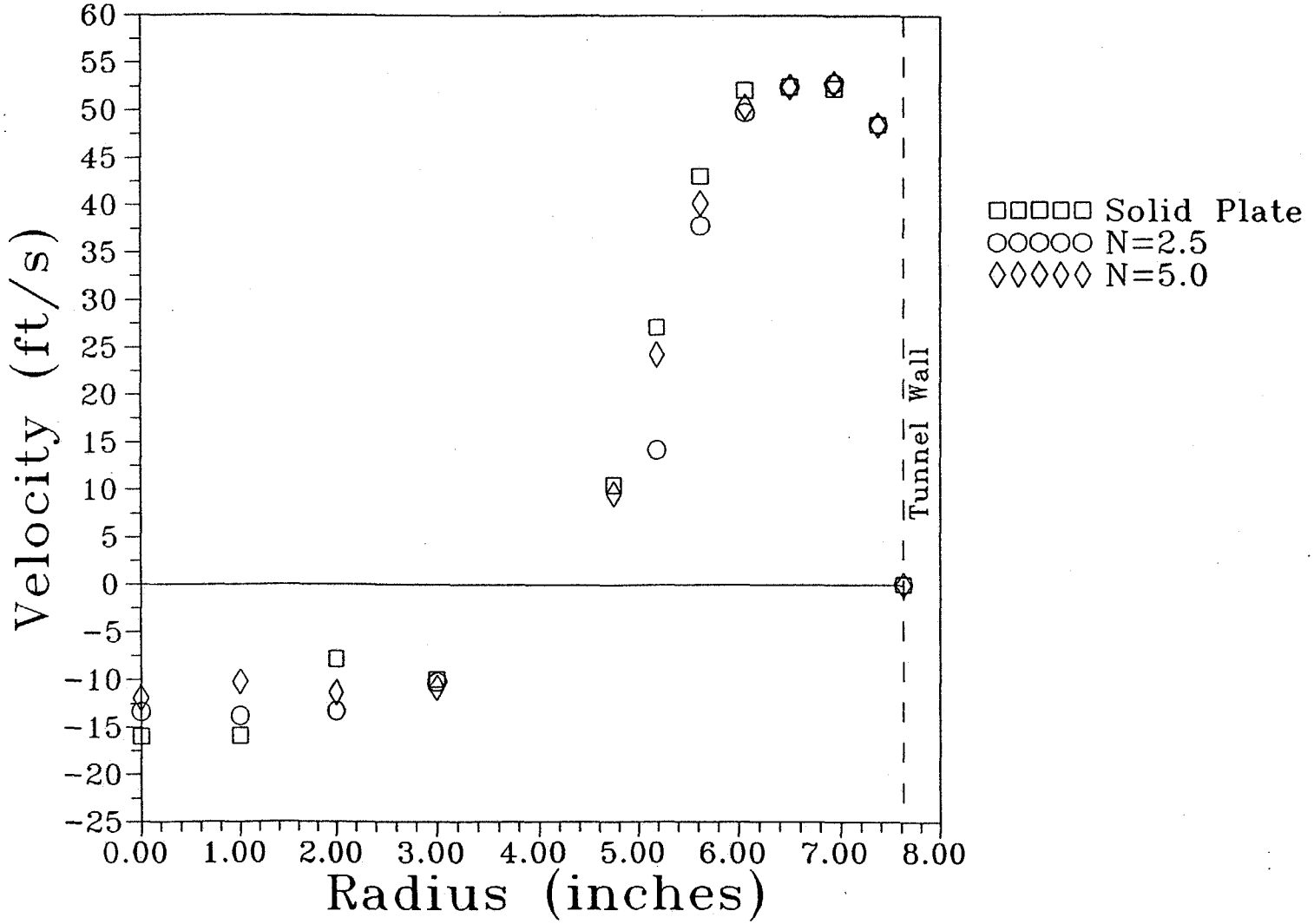

Fig. 26 Velocity as a function of radius for z/D = 0.40 at window C for various values of the base bleed ratio N

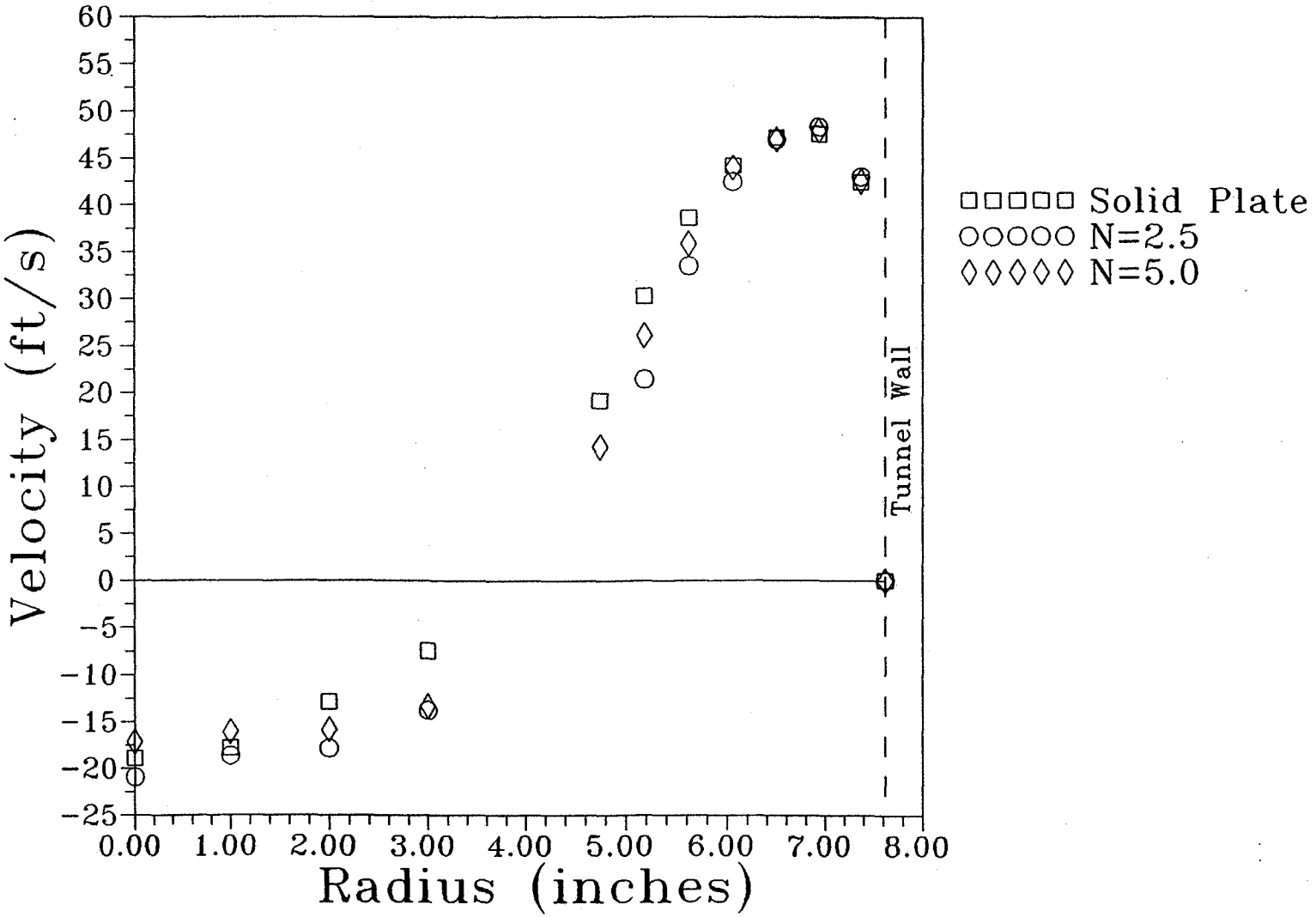

Fig. 27 Velocity as a function of radius for z/D = 0.82 at window C for various values of the base bleed ratio N

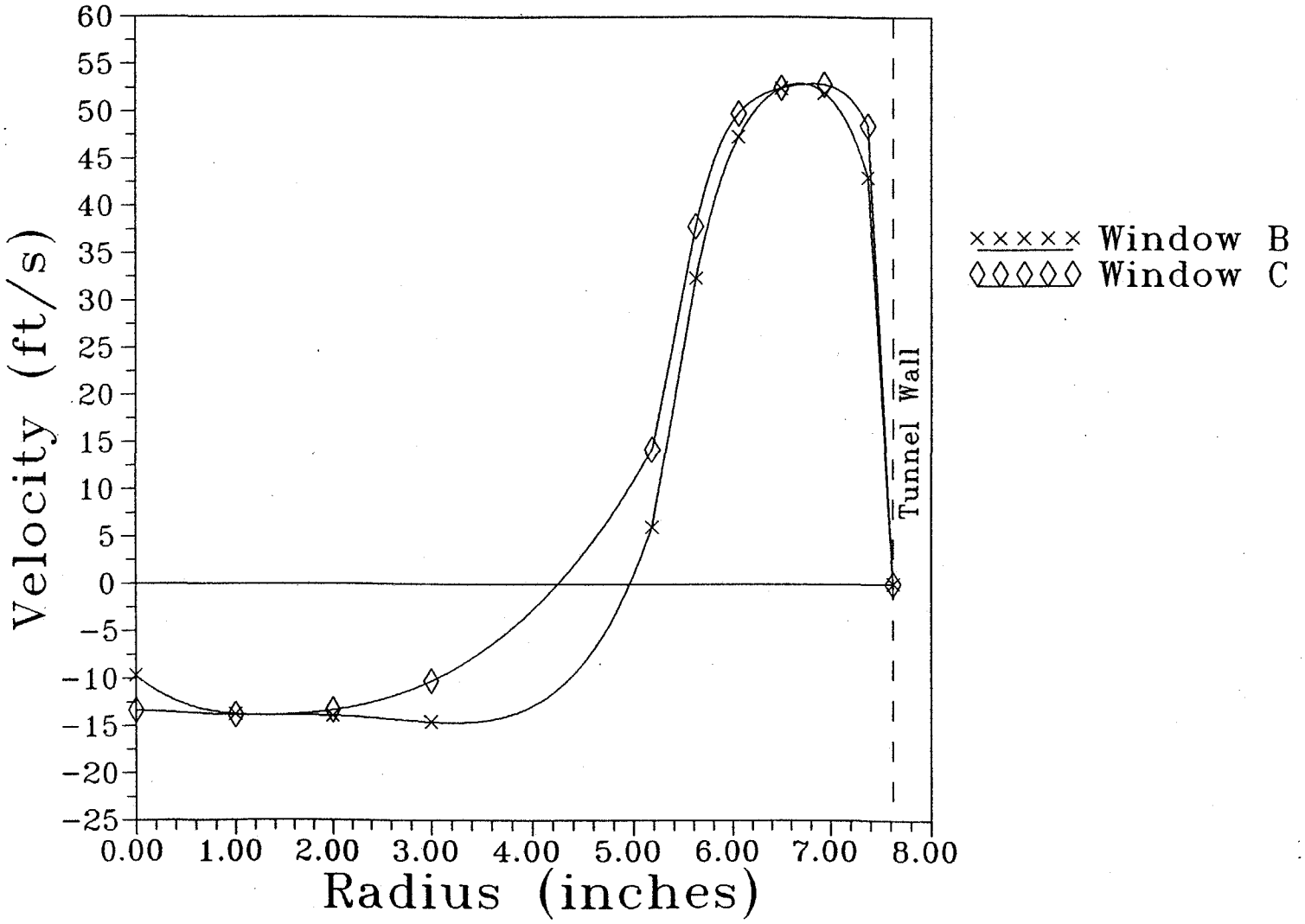

Fig. 28 Velocity as a function of radius for z/D = 0.40 at windows B and C for bleed ratio N = 2.5%. Curve fits added for clarity.

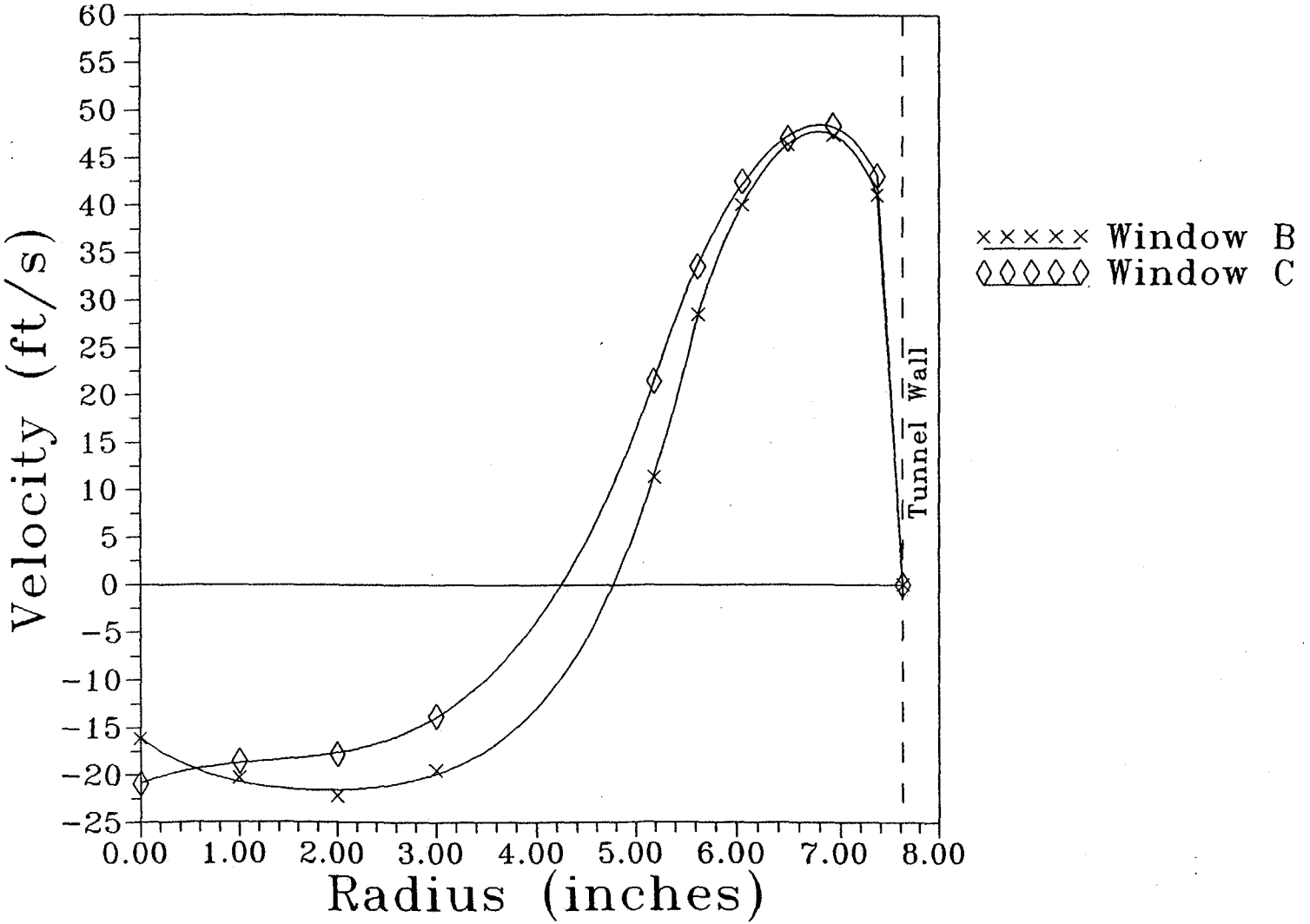

Fig. 29 Velocity as a function of radius for z/D = 0.82 at windows B and C for bleed ratio N = 2.5%. Curve fits added for clarity.

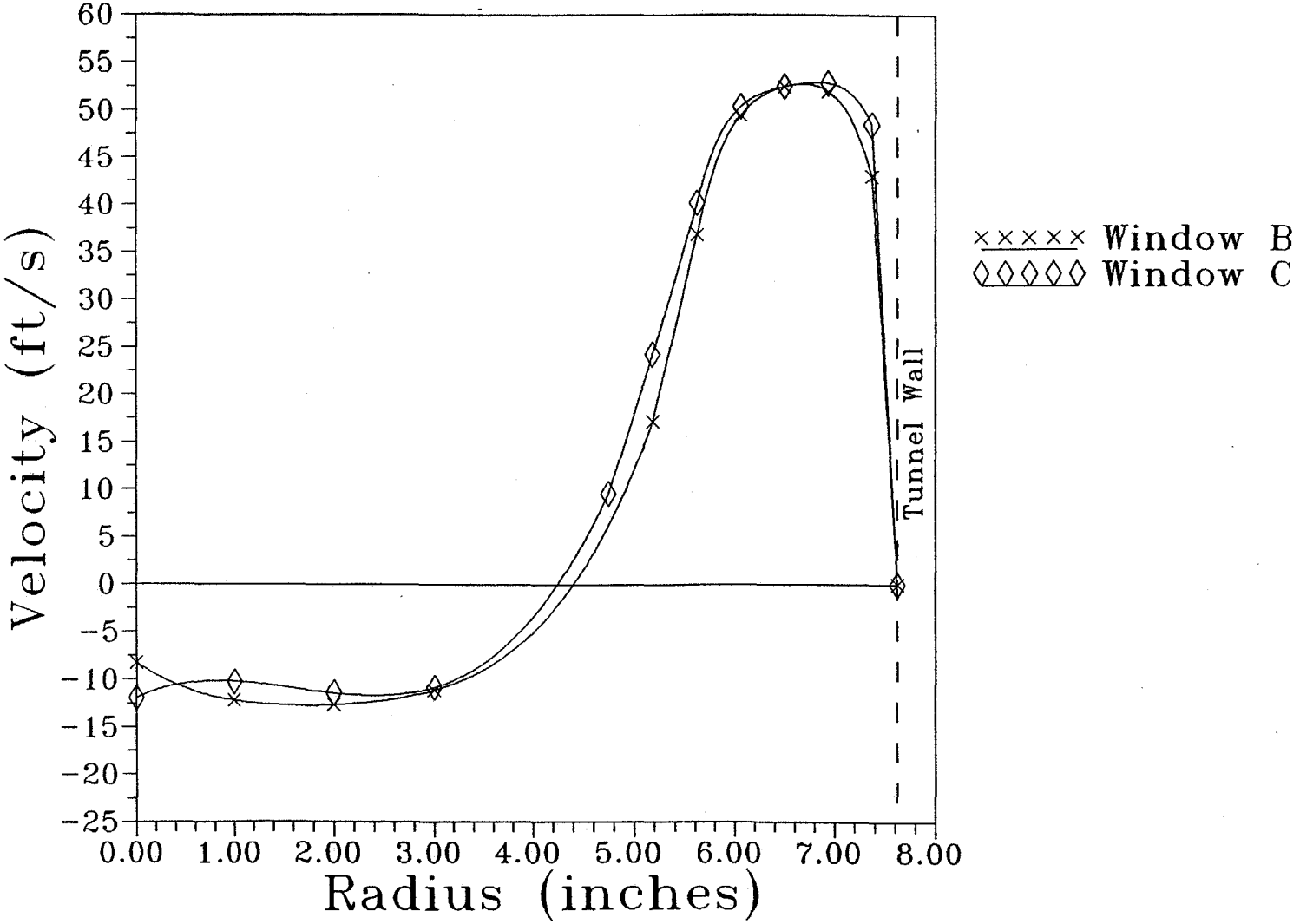

Fig. 30 Velocity as a function of radius for z/D = 0.40 at windows B and C for bleed ratio N = 5%. Curve fits added for clarity.

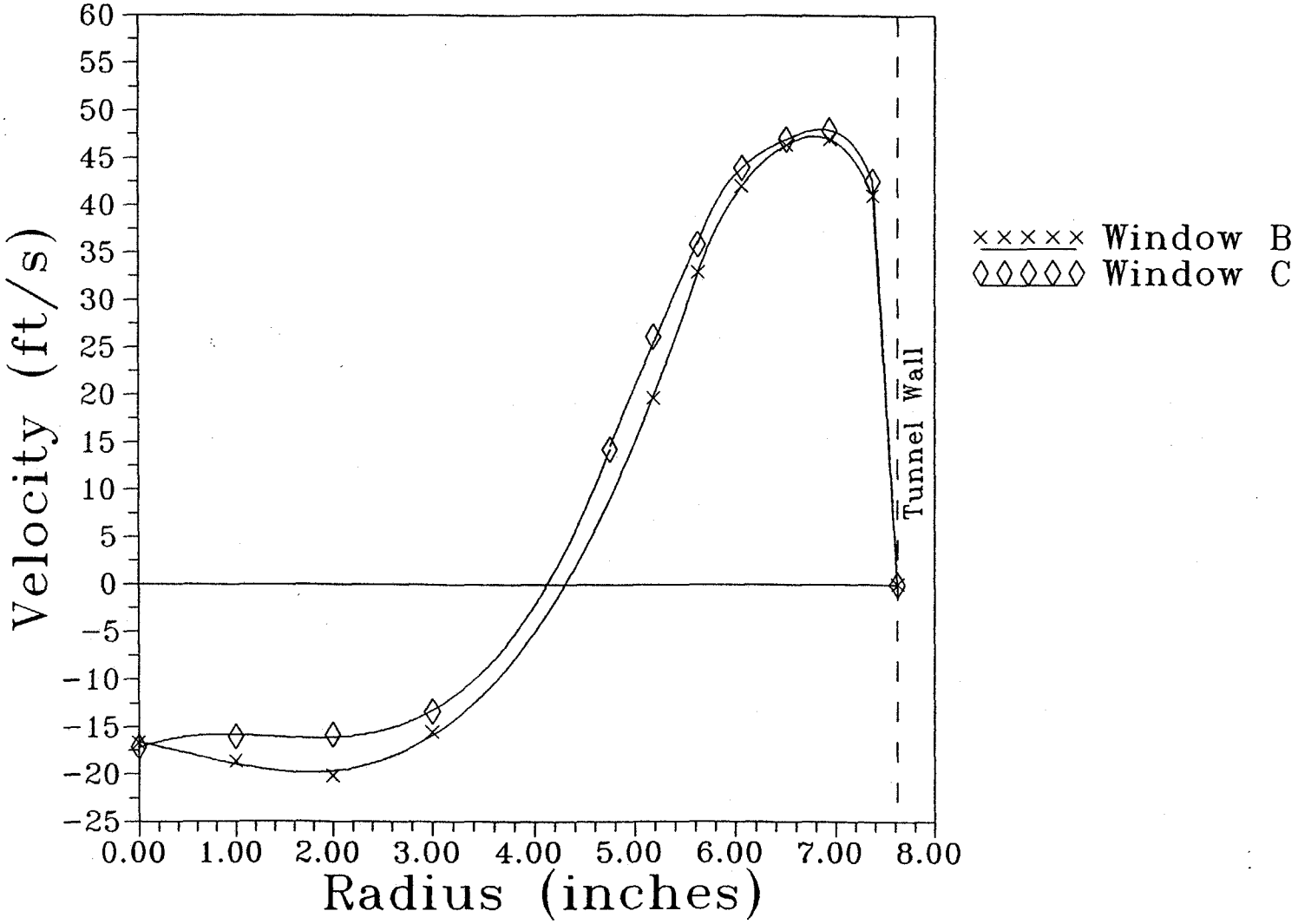

Fig. 31 Velocity as a function of radius for z/D = 0.82 at windows B and C for bleed ratio N = 5%. Curve fits added for clarity.

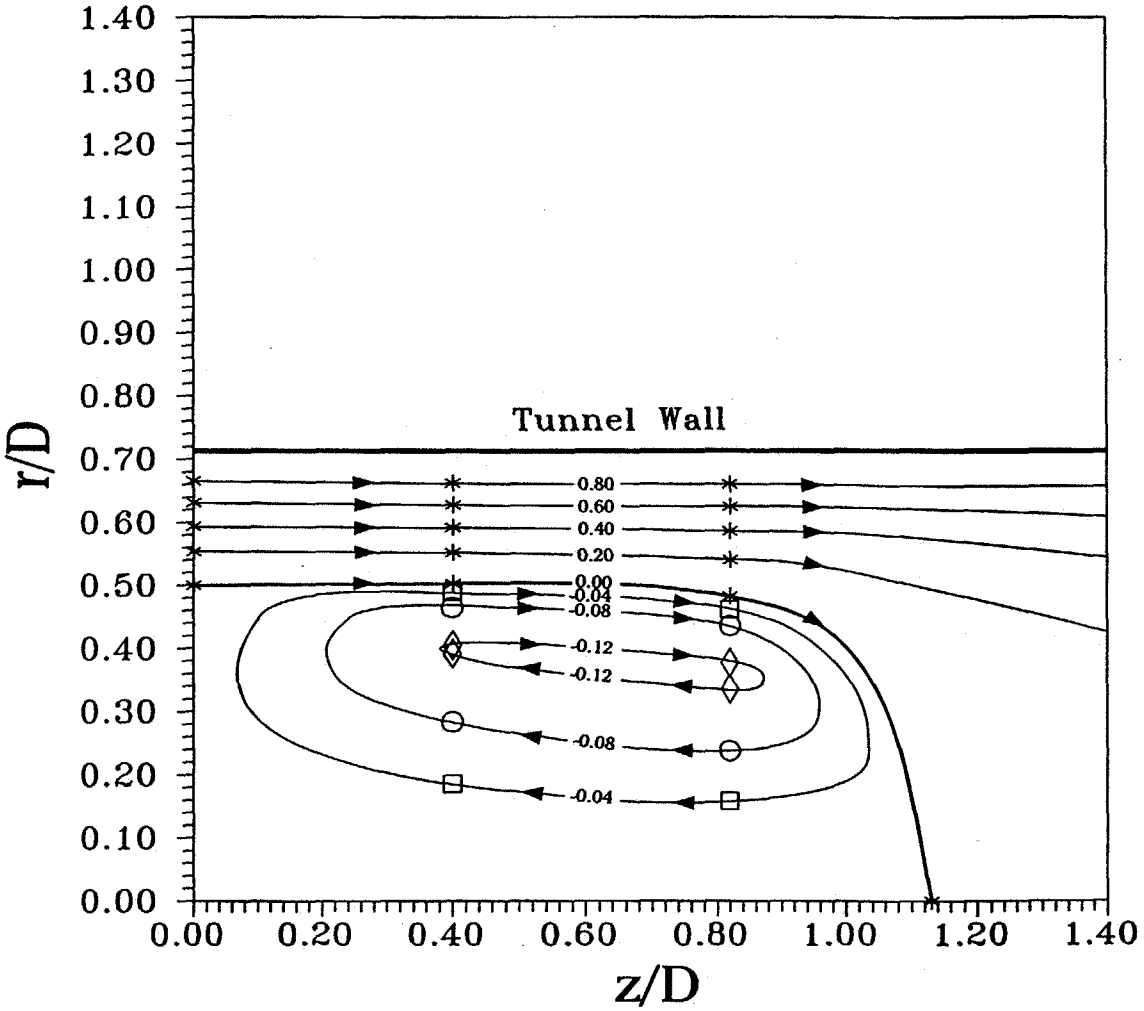

Fig. 32 Approximate streamline pattern in recirculation region for N = 0. Numbers on curves denote mass flow ratio m/m_{total}

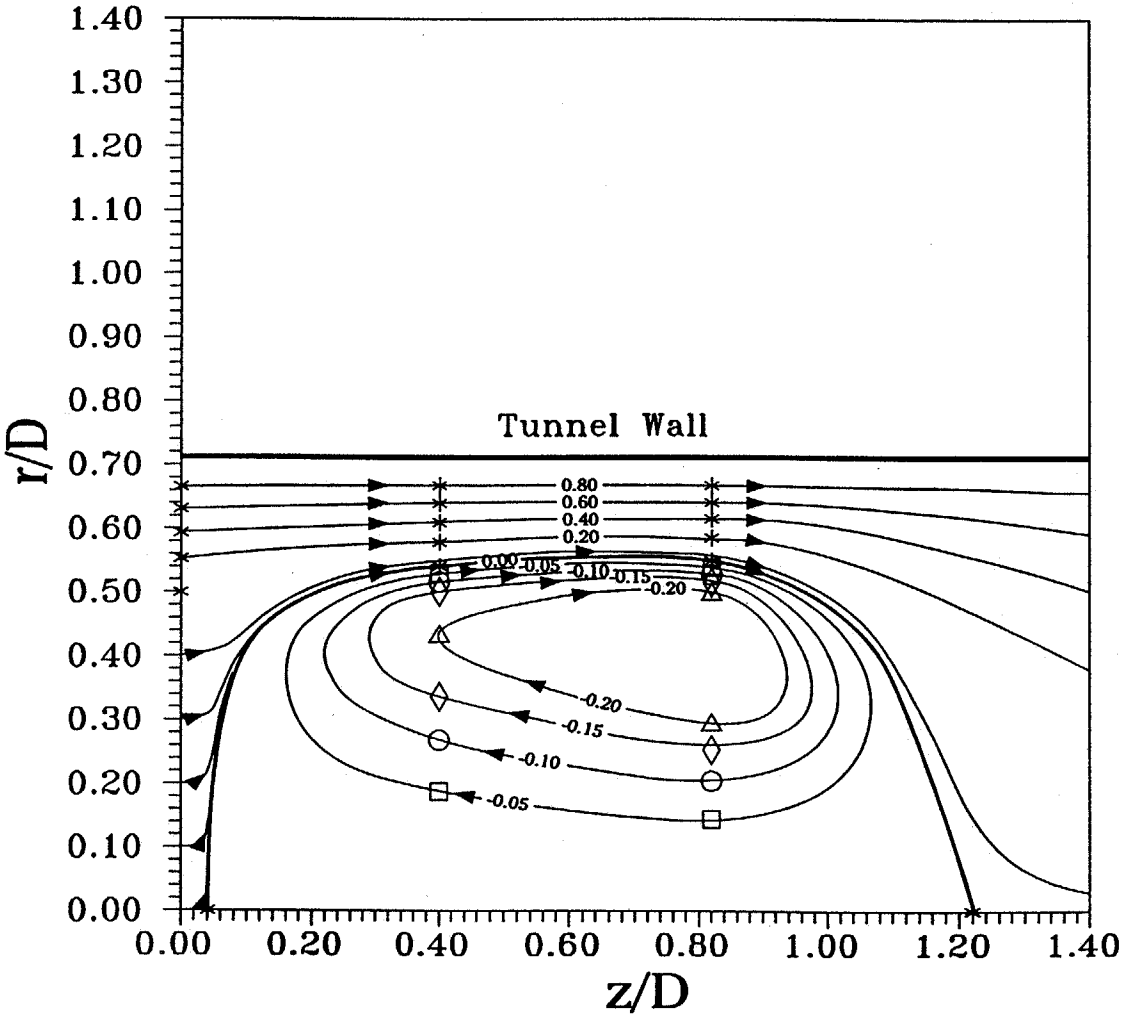

Fig. 33 Approximate streamline pattern in recirculation region for N = 2.5%. Numbers on curves denote mass flow ratio m/m_{total}

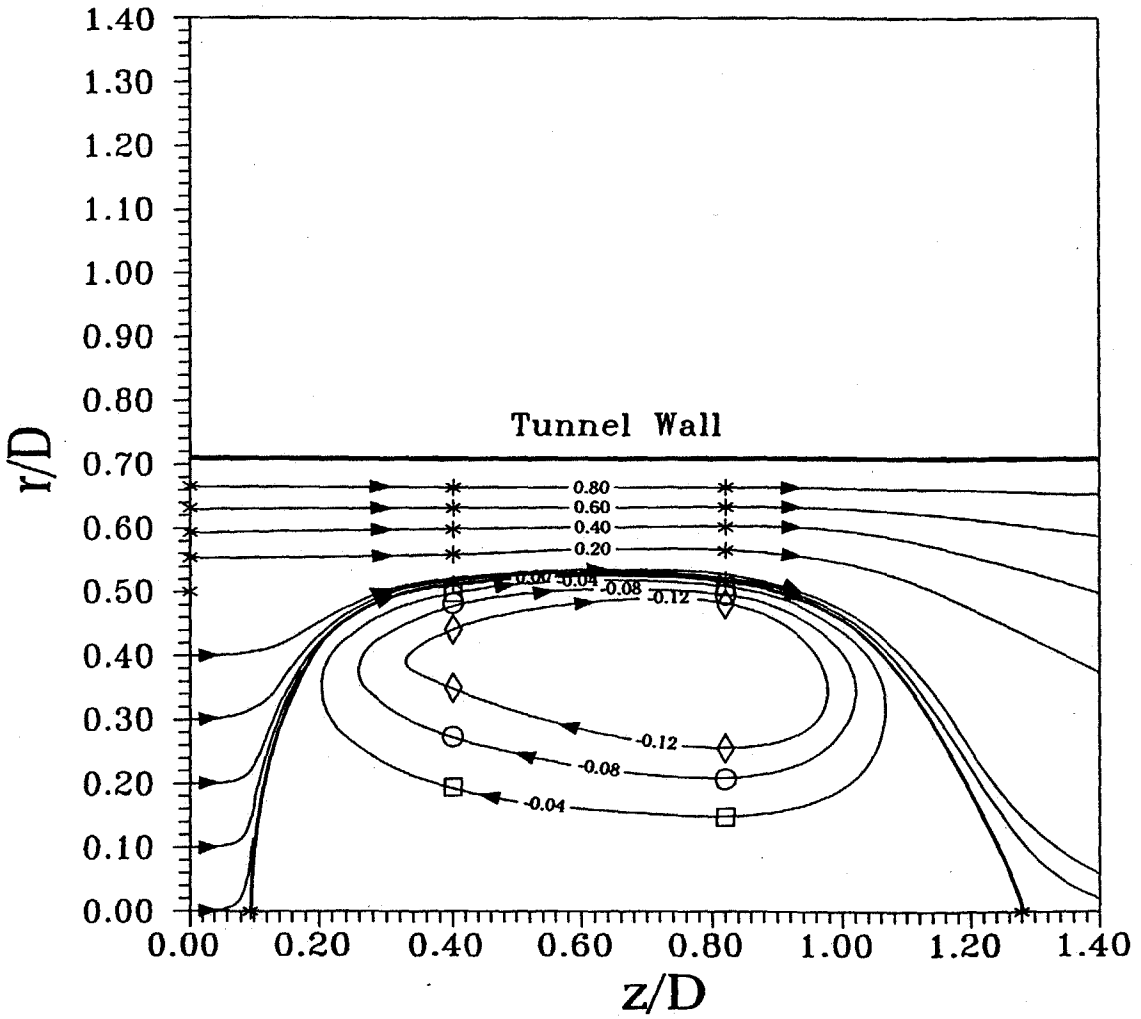

Fig. 34 Approximate streamline pattern in recirculation region for N = 5%. Numbers on curves denote mass flow ratio m/m_{total}

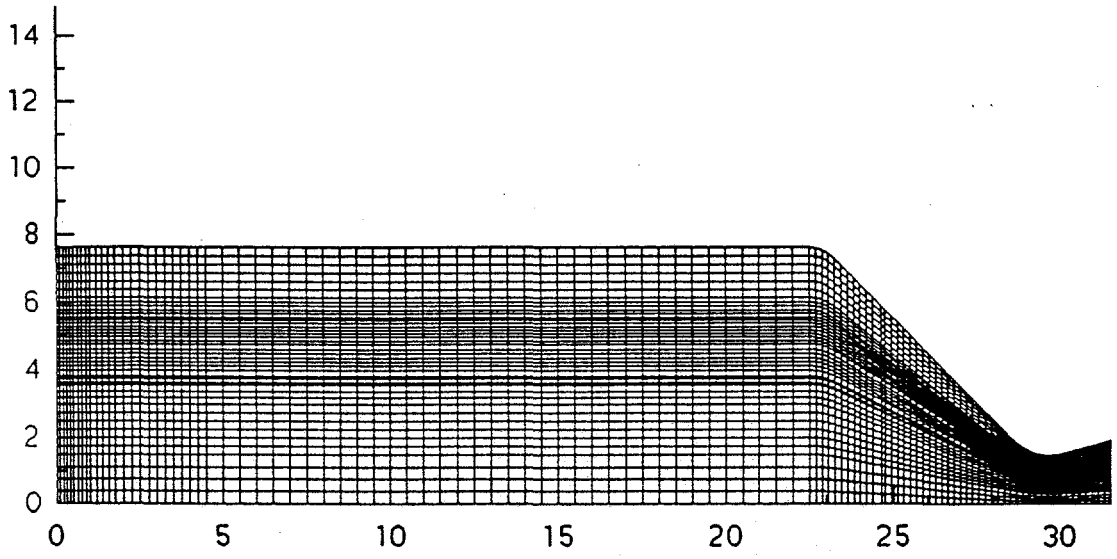

Fig. 35 Computational mesh used in the present study

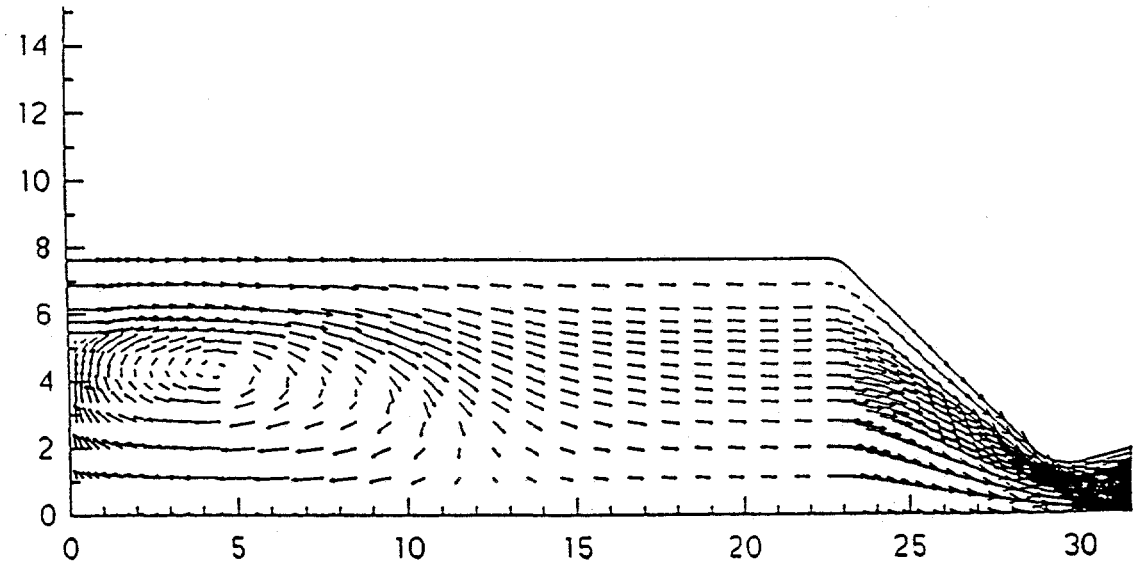

Fig. 36 Velocity vectors for base bleed ratio N =0

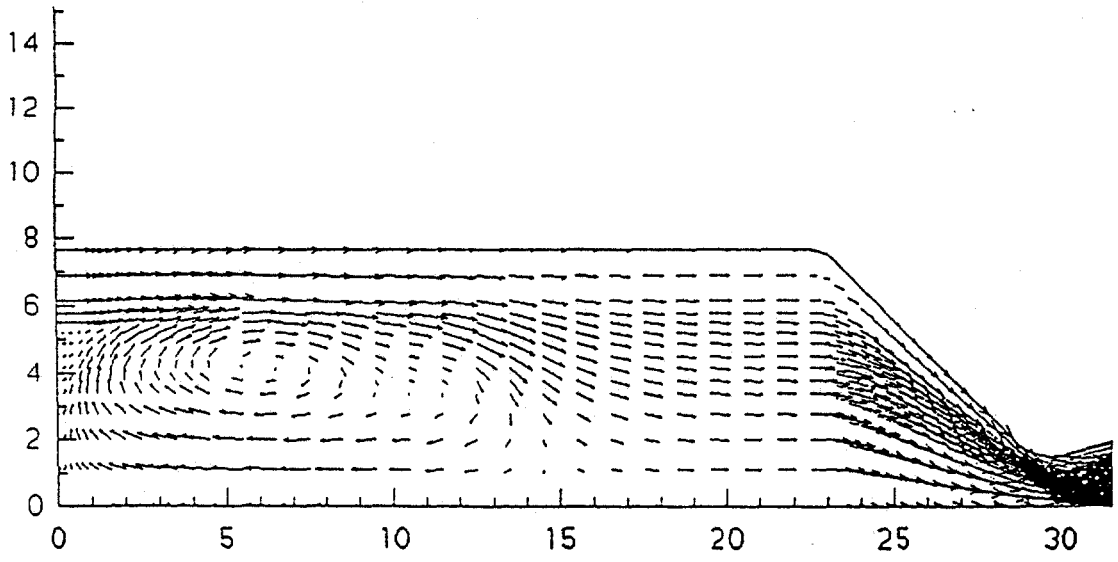

Fig. 37 Velocity vectors for base bleed ratio N = 2%

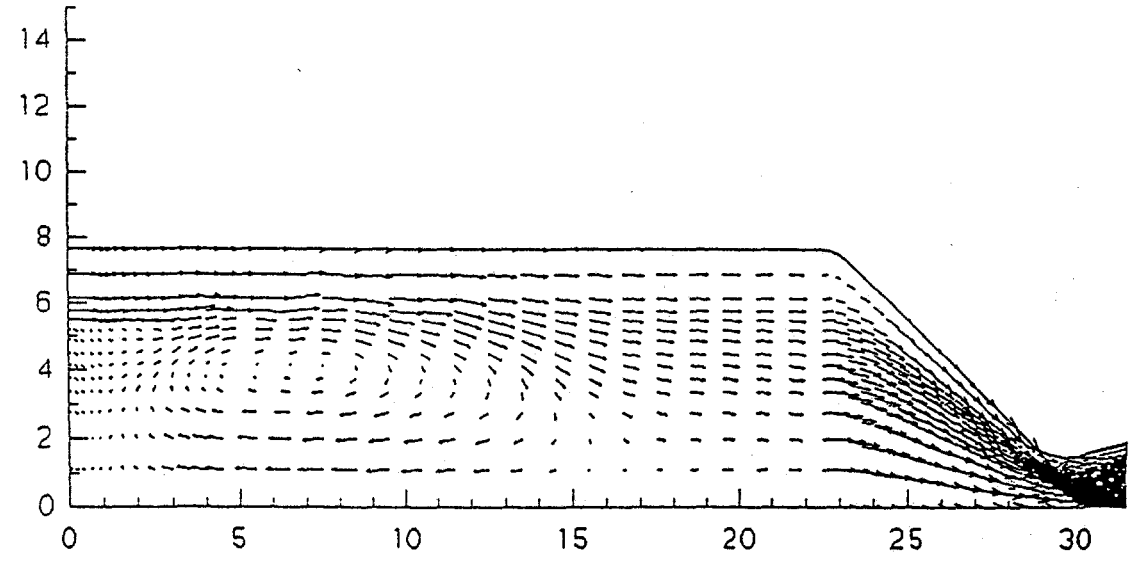

Fig. 38 Velocity vectors for base bleed ratio N = 5%